CRANFIELD UNIVERSITY

Maryam Ya-Alimadad

Study of Rate of Dust Build up on Optical Windows

School of Engineering
Department of Power and Propulsion

MPhil
Academic Year: 2011 – 2015

Supervisor: Dr D. Hammond
January 2016

CRANFIELD UNIVERSITY

School of Engineering
Department of Power and Propulsion

MPhil

Academic Year 2011 – 2015

Maryam Ya-Alimadad

Study of Rate of Dust Build up on Optical Windows

Supervisor: Dr D. Hammond
January 2016

ABSTRACT

The work presented in thesis is part of the DANIELA project which aims to replace the current air data system on civil aircrafts with a flush mounted Air Data System (ADS) built around a 3 axis Doppler LIDAR function as the primary data channel.

This thesis is focused on the comparison of different window materials and their optical clarity by means of theoretical and experimental analysis. Four different window materials including BK7, Sapphire, Germanium and ZnS are placed in a wind tunnel. The samples are each exposed to flows of air and water for specific periods of time during which temperature, pressure and air speed are recorded. Subsequently, each sample is carefully observed under the microscope. This is followed by the measurement of the amount of back scatter via detecting the change in the voltage once it is placed in the optical station.

The optical tests reveal the amount of dust adhered to the samples which results in increased voltage. Review of these samples under the microscope matches the results obtained from the optical test. The two sets of data obtained from the two tests determined that some samples collected more dust in comparison to others. It was established that under identical test conditions i.e. flow, temperature and moisture, BK7 and Sapphire collect considerably less dust compared to ZnS. Moreover it was impossible to test Germanium sample optically, under a microscope as it is a dark opaque glass.

Keywords:

Adhesion, Icing Tunnel, Bounce, Detachment, Aerosols

ACKNOWLEDGEMENTS

I would like to express my gratitude to the following people for their support guidance and advice during this project.

- Dr. David Hammond for his advice, guidance and assistance.
- Dr Joao Amaral Teixeira for his assistance.
- Professor Hoi Yeung and Professor Mike Reeks for their help and advice.

Finally, I must express my thanks to my sister, parents and my brother in law for providing me with unfailing support and continuous encouragement throughout my years of study and through the process of researching and writing this thesis. This accomplishment would not have been possible without them. Thank you.

TABLE OF CONTENTS

LIST OF FIGURES

LIST OF TABLES

LIST OF ABBREVIATIONS

ADS	Air Data System
AOA	Angle of Attack
CFD	Computational Fluid Dynamics
DANIELA	**D**emonstration of **AN**emometry **I**nstrum**E**nt based on **LA**ser
LIDAR	Light Detection And Ranging
SSA	Side Slip Angle
TAS	True Air Speed
ZnS	Zinc Sulphide

CHAPTER 1. INTRODUCTION

The aim of DANIELA (Demonstration of Anemometry InstrumEnt based on Laser) is to replace the current typical air data system which is composed of probes and pressure sensors, with a flush mounted Air Data System (ADS) built around a 3 axis Doppler LiDAR (Light Detection And Ranging) function as the primary air data channel on a civil aircraft. This will include the Doppler related functions such as True Air Speed (TAS), Side Slip Angle (SSA), Angle of Attack (AOA) and also the measurement of temperature and density.

The existing system has provided sufficient precision however it suffers from lack of robustness against bird collision, passenger (stair mishandling) or hailstone.

In addition, to ensure the system availability, the probes need de-icing; this requires high power consumption (typically 9,000 Watts for the 3 air data channels). Furthermore, for safety purposes they require high levels of maintenance as the externally mounted probes are exposed to corrosion.

There is also a higher risk of failure as both primary and standby channels may have similar failure modes. Therefore, using a laser-based system will reduce the system malfunction by reducing the probability of common failures. (TEEM Photonics – 2008)

The DANIELA mock up is a flyable, 4-axis, Very Short Range Infra-Red Dopler LiDAR. The mock up operates at 1.5µm, with 1W laser power on each axis. Its optical architecture has been optimised to accomplish the “shot noise” limited operation. This results in achieving the highest signal to noise ratio with the lowest emitted laser power.

DANIELA project is divided into different work packages. One of which is the windows research and development. This package consists of research into maintenance and improvement of the optical window material. The project includes comparing the dust build up on a series of different window materials by means of optical clarity.

The DANIELA project came to an end in January 2012. However, sections of the research are still on-going. This includes the research into windows.

1.1 Study Objectives

The work presented in this thesis is focused on the comparison of different window materials and their optical clarity by means of theoretical and experimental analysis. In general, the project aims to establish whether some materials collect more dust in comparison with other materials, under identical conditions.

The Detailed objectives of the project are to:

- Carry out a detailed review of literature on the behaviour of particles when they come into contact with a surface.
- Perform hand calculations and numerical analysis, and use existing numerical results to understand the behaviour of particles and surfaces as they come into contact with each other.
- Design and develop a test rig for the purpose of the comparison of materials in collecting dust.
- Perform an experiment with an existing icing tunnel to compare the amount of dust adhering to different materials
- Carry out optical tests to compare the amount of dust built up on selected optical windows

1.2 Outline of Thesis

The framework of this thesis is as follows:

After this introduction, chapter 2 provides a comprehensive review of literature on the definition of Aerosols, their shape, size, and concentration. It also looks at forces acting on particles in contact with surfaces and interaction of light with suspended particles.

Chapter 3 focuses on the techniques corresponding to the experimental set-up stages of the work, as well as those related to the methodologies involved in obtaining the experimental data and the post-processing and analysis of the results. It also includes the background theories and formulations on the behaviour of fluid flow in pipes and on smooth surfaces; as well as the theoretical background related to the selection of different materials for the windows. This chapter also introduces the experimental and numerical methods used throughout the project. It includes the calculations carried out in the design of the test rig.

Chapter 4 provides the details of the experiments carried out on window samples placed inside an icing tunnel, the results achieved and their analysis followed with the background theory.

Chapters 5 and 6 outline the conclusions and recommendations for future work, respectively

CHAPTER 2. LITERATURE REVIEW

In line with the main objective of this project, which is to compare the effect of particle adhesion on selected window samples, it is important to understand the behaviour of surfaces and aerosol particles when they come into contact with each other. Prior to doing that, it is important to review the definition of aerosols and their characteristics.

This chapter starts by providing a review of literature on the definition of Aerosol in Section 2.1. The chapter then continues by looking at Aerosol particles' shape and size and concentrations of aerosol particles in the atmosphere, in Sections 2.2, 2.3 and 2.4, respectively. It then brings to focus different factors influencing the behaviour of aerosol particles when they come into contact with a surface in Section 2.5. Finally, Section 2.6 discusses the interaction of light with suspended particles.

2.1 Aerosol Definition

Aerosols are formed either by gases changing into particulate matter or by the disintegration of liquids or solids as explained by Friedlander (1977). They may also be formed from the re-suspension of powdered material or the break- up of agglomerates as described by Hinds (1982).

Vincent (1989) defines aerosols as a disperse system of liquid or solid particles suspended in a gas, usually air. Examples of these can be divided into two groups; naturally occurring ones such as snowstorms, sandstorms, mists, clouds, etc, or man-made ones including smoke, fume, coal dust, cement dust, asbestos dust, etc. Aerosols can also be divided into two other categories as explained by Hinds (1982): primary aerosols which consist of particles introduced directly into the atmosphere, and secondary particles which are created in the atmosphere as a result of the chemical reaction of gaseous components (gas to particle conversion).

Reist (1984) defines dust as solids created by processes such as crushing, grinding, blasting and drilling. These particles are the same as the parent

material only smaller, with the sizes ranging from sub microscopic to microscopic.

In a report written by Christopher Ritter (2009) for DANIELA, six main categories of aerosols have been named. These categories are: 1) urban-polluted 2) biomass burning 3) desert dust 4) sea salt 5) volcanic dust 6) Arctic haze (a unique aerosol feature which occurs over the otherwise pristine Arctic.)

Particle size, concentration and chemical composition of the aerosol particles are usually the most influential characteristics of the particles on human health, visibility and climate. Light scattering is one of the effects which are dependent on the size of the particles. Figure 2.1 by Friedlander (1977) shows the light scattered per unit mass of aerosol versus particle diameter for wavelengths in the visible range. This shows that the maximum scattering efficiency corresponds to the particle size of the same order as the wavelength of the incident light.

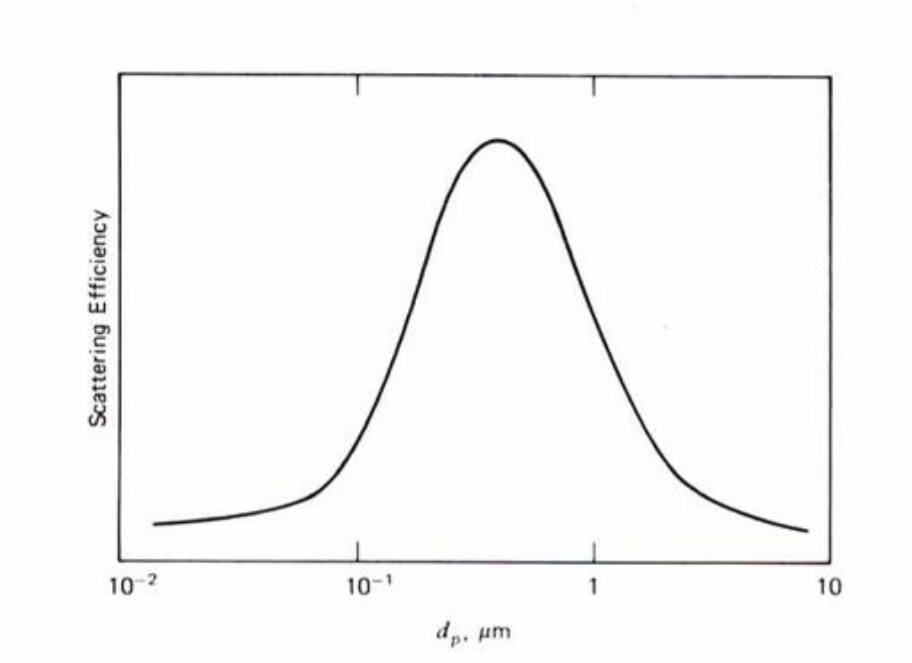

Figure 2.1 - Light scattering efficiency, expressed as light scattered per unit mass of particles. The peak occurs in the range corresponding to the wavelength of the scattered light in the visible range.

2.2 Shape

For ease of calculation the aerosols are often assumed to be spherical. This also helps with the visualization of the processes taking place. However, with liquid droplets always being spherical, as an exception, many shapes are possible as explained by Reist (1984). These shapes can be divided into three categories:

- Isometric particles: these have all their three dimensions as equal. Spherical, regular polyhedral and particles approximating these shapes are part of this group.
- Platelets: these are particles which have two long dimensions and a small third dimension. This group includes leaf fragments, scales, and disks.
- Fibres: they are particles with great length in one dimension compared to a much smaller length in two other dimensions. Examples of this group are prisms, needles, threads or mineral fibres such as asbestos.

2.3 Size

According to Hinds (1982), one of the most significant parameters, for characterizing the behaviour of aerosols is the particle size.

Assuming that the aerosol particles are spherical; the particle radius or the diameter can be used to describe particles sizes. Aerosol particle sizes range from 0.001μm to 100μm. According to Figure 2.2, Hinds (1982), dusts, ground materials and pollen are in the micrometre range or larger and fumes and smokes are sub-micrometre or smaller.

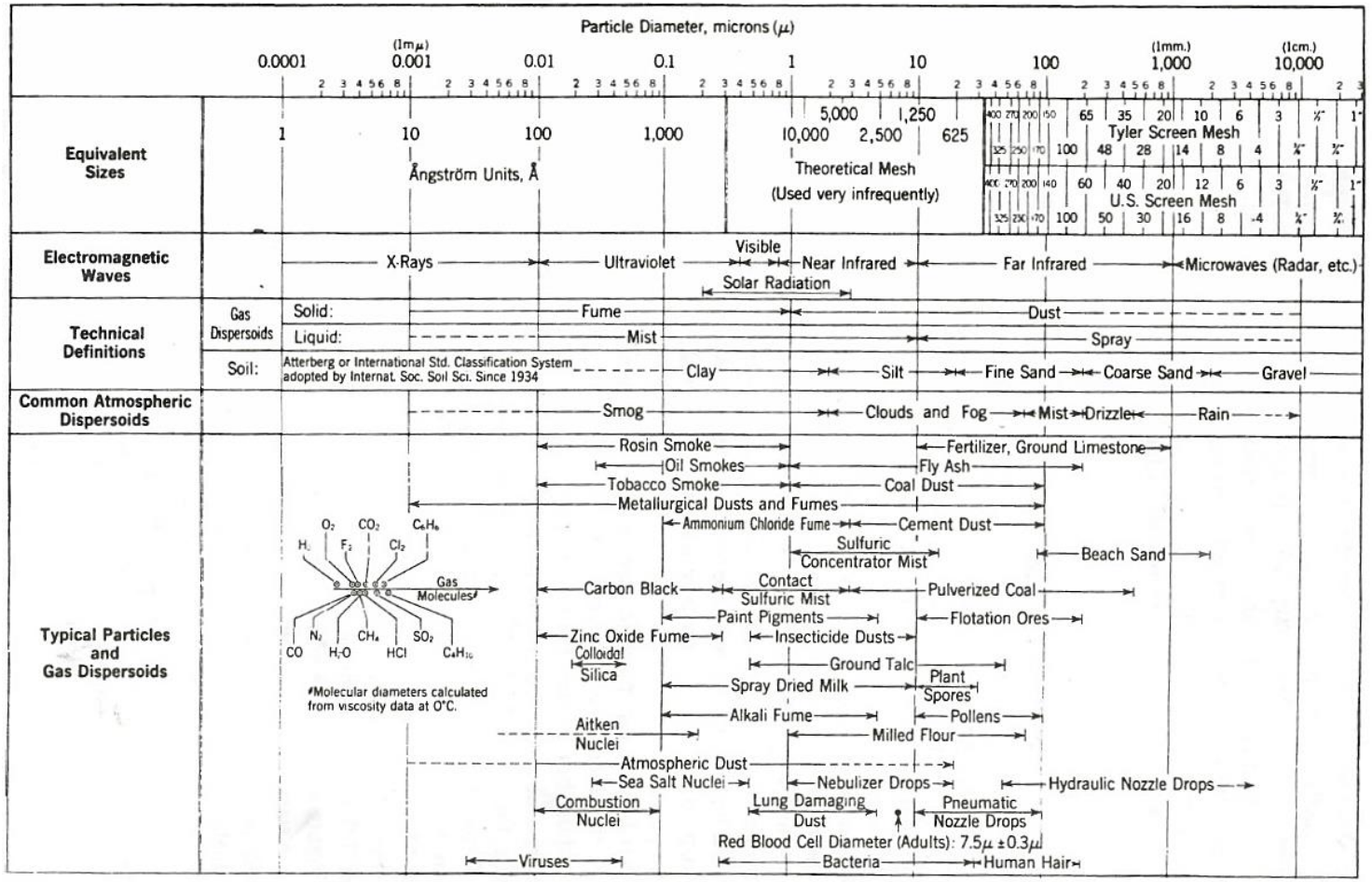

Figure 2.2 - Particle size range for aerosols.

2.4 Concentration

Another property of aerosol particles is their mass concentration (c), which is defined as the mass of particulate material in a unit volume of gas, i.e. air. Aerosol concentration is important to this study, as low aerosol concentration could challenge the LIDAR system on board the aircraft and the high aerosol concentration and extreme storms may result in reduced flight safety.

Ritter (2009) reports that various studies have shown, aerosol concentrations above the ocean are lower than over the land, or more accurately air whose path had never been in contact with any continent clearly show a lower aerosol content.

Carlson and Benjamin (1980) consider wind-blown dust as one of the dominant aerosols in the lower atmosphere; this is mostly composed of mineral particles together with some organic matters. Although they are fairly large, with consequently high settling rates, under some conditions these dust particles can spread far from their source and remain in the atmosphere for long periods. A notable example is dust from the Sahara, which spreads across much of the Atlantic Ocean between Africa and the Caribbean during summer months.

Bohren and Huffman (1940), explain that dominating the marine aerosol are salt particles, together with some organic particles of marine origin. The globally dominant mass of particles, found distributed over the entire earth, is composed of sulphur compounds, including ammonium sulphate, and sulphuric acid. These particles are formed mostly in the stratosphere by complex chemical reactions. In periods of strong volcanic activity, volcanic ash maybe significant; volcanic ash remains in the atmosphere for several years after its introduction. Minor constitutes of the atmospheric aerosols include terrestrial organic substances such as terpenes and pollution such as carbon, metal oxides and photochemical smog.

Friedlander (1977) describes the concentration of aerosols as follows:

Assuming δN is the number of particles in an initially rather large volume δV surrounding the point P in the gas, the average (number) concentration of the particles within the volume δV, is the ratio of $\delta N/\delta V$. Depending on the concentration gradient in δV, the average concentration can either increase or decrease as δV shrinks towards the point P. However, the concentration gradient will generally approach a constant value over a range of values of δV in which the gradient is small but many particles are still present. This constant value is the particle concentration at the point P. As the volume continues to shrink, the number of particles becomes so small that the average concentration fluctuates randomly in space and time, i.e. it is not statistically stationary.

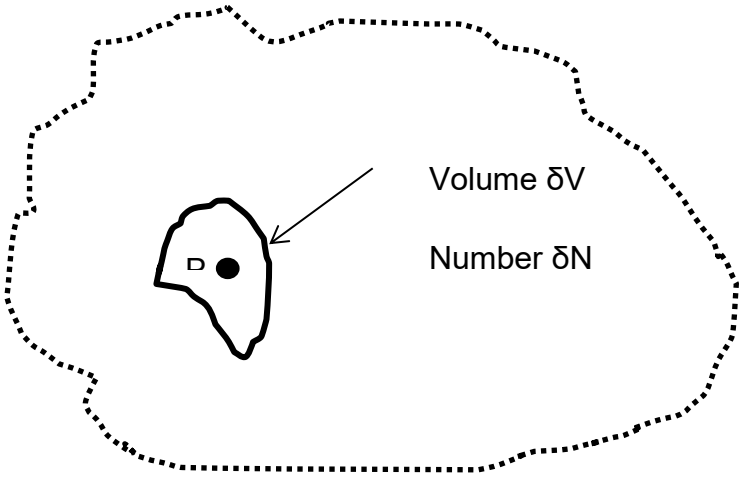

Figure 2.3 - The volume δV contains δN particles shrink toward point P

2.5 Forces Acting on Particles in Contact with Surfaces

To study the behaviour of aerosol particles, just knowing the size of the particle will not be sufficient. Effects of the aerosol particles, such as mass and electrical charge plus the properties which are joint properties of particle and the medium, such as diffusion coefficient and sedimentation speed are all the factors which need to be considered in order to achieve reasonable findings.

But firstly the behaviour of both the particle and the surface when they come into contact with each other needs to be considered. Small particles may or may not stick to surface depending on their collision velocity as described by Esmen et al (1978). Low collision velocity results in the particle adhesion to the surface whereas high collision velocity results in particle bounce.

Bowden and Tabor (1958) divides the impact between a solid particle and a solid surface into four stages. When a solid particle comes into contact with a solid surface at stage one the region of contact is deformed elastically. If the contact is smooth, the surface recovers elastically and separates with no deformation occurring.

The second stage is when a slight plastic deformation occurs and stage three occurs when the impact energy is higher and complete plastic deformation occurs in the surface. The plasticity will reach full scale until the whole kinetic energy of the particle is consumed. Finally at stage four elastic stresses in both surfaces are released. This results in particle rebound. Note that this process has been described for solid particles of approximately 1cm diameter coming into contact with a solid surface. However the same can be said about particles of smaller diameter, this is explained by Esmen et al (1978).

Esmen et al (1978) describes the process for particles of much smaller diameter of between 4.4 to 15.5μm when they come into contact with a smooth solid surface. The particle surface collision is regarded as the energy of the particle-surface system. Esmen et al (1978) describes this system as a potential well, in which the particles with low rebound energy will be captured by the surface, when they are near it. During the collision the depth of this potential well can alter, if the particle is charged, permanent or transient deformation in the particle and surface occurs.

Apart from particle adhesion and particle bounce as described in this section, other effects which should be taken into account for the purpose of this thesis are the particle bounce, detachment and re-suspension from the surface. This is explained in details in sections 2.5.2, 2.5.3 and 2.5.4 of the thesis.

2.5.1 Adhesion of Particles

Dust particles have a great tendency to cling to surfaces such as leaves, fabric, and walls. This shows that gravitational and aerodynamic forces can fail to overcome the adhesion forces of these particles. It also implies that applying external forces such as air flow does not remove all the particles.

Hinds (1982) explains that the main adhesive forces on a particle are London Van der Waals, electrostatic forces, and the surface tension of adsorbed liquid films. These forces are affected by the material properties, roughness, contamination of the surface; relative humidity, temperature, duration of contact and initial contact velocity.

Additionally, Zimon (1969) explains that the number of dust particles adhering to a plate placed into a flow of air depends on the concentration of aerosol particles in the flow, properties of the dust and the surface and the arrangement of the surface according to the axis of flow.

London Van der Waals Forces

Corn (1961) and Friedlander (1977) define London Van der Waals Forces as the force by which the molecules or atoms of different material or compositions are attracted to each other. These forces are effective at short distances and they reduce to zero as the distance increases. They result from fluctuations in the electron clouds surrounding the nucleus. Electrically neutral and symmetric atoms or molecules have instantaneous dipoles. These dipoles induce dipoles in the neighbouring atoms or molecules. This is shown in Figure 2.4.

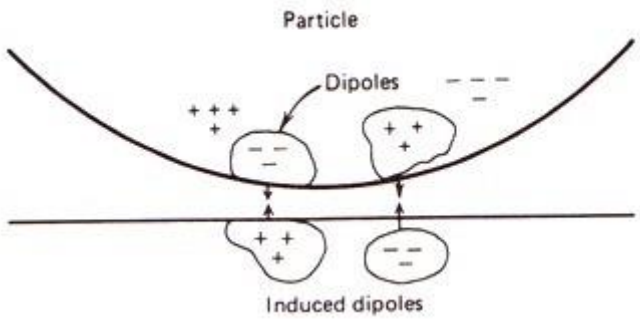

Figure 2.4 - Van der Waals adhesive force

The surfaces of most materials are irregular as explained by Hinds (1982). The initial contact between the particle and surface happens only between a few asperities as shown in Figure 2.5. After initial contact, the asperities are gradually deformed by Van der Waals forces and the separation distance between the particle and the surface is reduced. This increases the contact area until balance is restored between the attractive forces and the forces resisting deformation. The deformation process may take as long as a few hours. The hardness of the materials involved controls the size of the ultimate area of contact and consequently, the strength of the adhesive force.

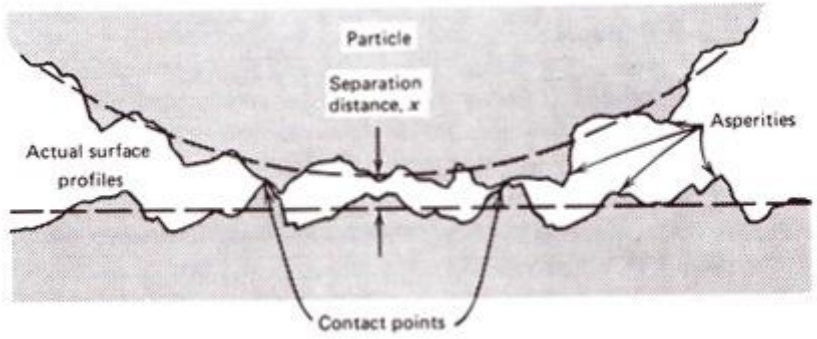

Figure 2.5 - Sub microscopic contact geometry

Effects of Relative Humidity on Adhesion

Various experimental studies carried out by different scientists such as Bowden and tabor (1954), Ranade (1987) and Corn (1966); show that the relative humidity of the ambient air affects the adhesion of solid particles to solid surfaces. Adhesion force generally increases with relative humidity.

Figure 2.6 and Figure 2.7 by Corn (1966) demonstrate the effects of relative humidity on adhesion of quartz particles to Pyrex and glass particles to quartz, respectively.

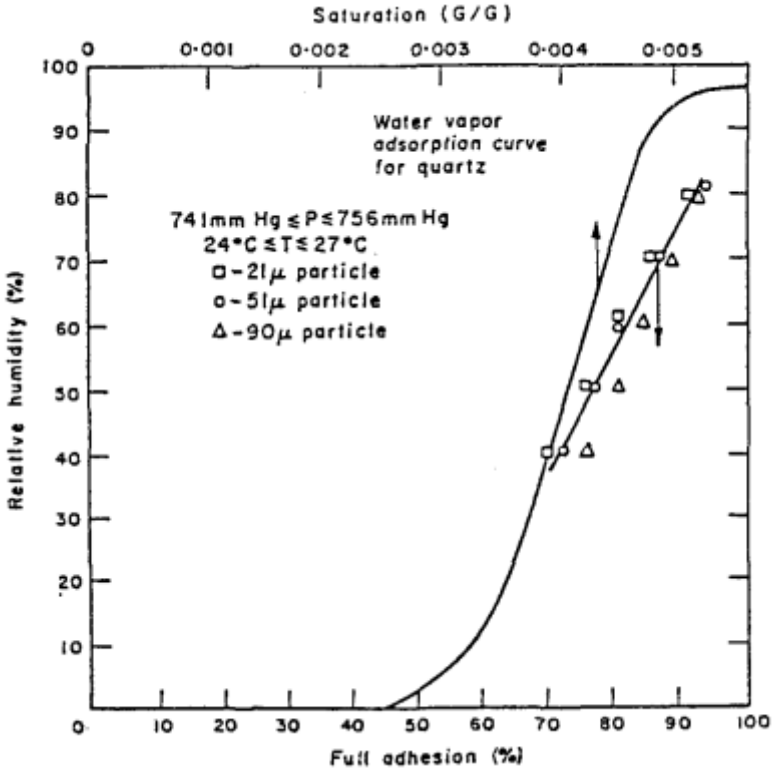

Figure 2.6 - Adhesion of quartz particles to Pyrex

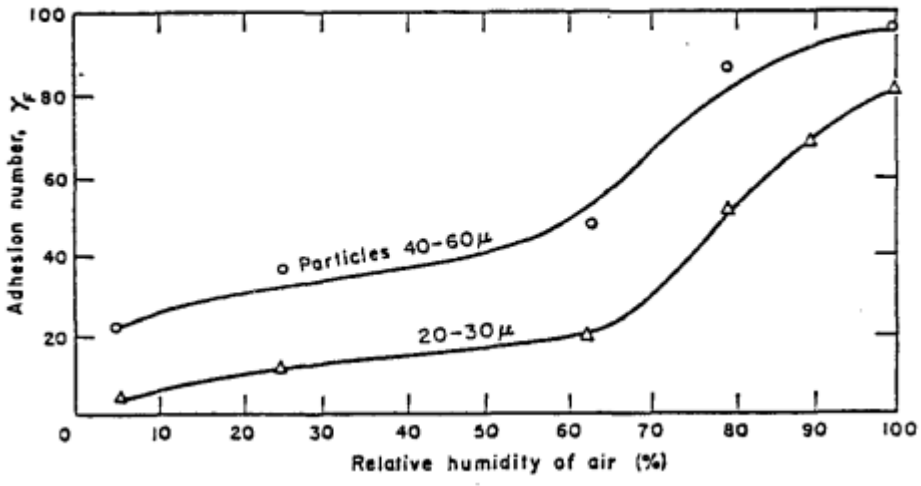

Figure 2.7 - Adhesion of glass particles to quartz

Effects of Surface Roughness on Particle Adhesion

Analytical results obtained by N.B. Wood (1980), on turbulent deposition to smooth and rough surfaces, suggest that the deposition rates are greatly affected by the surface roughness.

Yakov et al. (2000) explains that the nanoscale surface roughness dramatically reduces adhesion between a particle and a surface. This is caused by the reduction in real area in contact and increase in the distance between the bulk surfaces.

Effects of Static Electricity on Adhesion

Most aerosol particles carry some electric charge and some may be highly charged. As a result for highly charged particles, electrostatic force can become greater than gravity.

2.5.2 Particle Bounce

Hinds (1982) and Esmen (1978) explain that when a particle contacts a surface at high velocity, part of the kinetic energy is transformed into the deformation process (plastic deformation), and part of it is converted elastically to kinetic energy of rebound. The particle will rebound and bounce away from the surface if the rebound energy exceeds the adhesion energy. Bouncing depends on particles and their sizes. It does not occur for droplets or easily deformed particles such as tar. The harder the particle material, the larger the particle or the greater its velocity, the more likely bounce is to occur, although surface roughness plays a significant role. Coating surfaces with oil or grease increases the adhesion energy, the deformation and the dissipative energy. They also greatly reduce the possibility of bouncing.

2.5.3 Detachment

Some aerosol particles adhere to the surface as they come into contact with the surface. However, these can then be removed from the surface if sufficient removal force is applied. Hinds (1982) explains that adhesive forces are proportional to the particle diameter (d) whereas the removal forces are

proportional to d^3 for gravitational, vibrational, and centrifugal forces and d^2 for air currents. Based on this relationship, it becomes more difficult to remove the particle from the surface as the particle size decreases. On the other hand, larger particles and visible particles such as grains of sand can be removed more easily by shaking or air currents. Smaller particles such as soot particles are not able to do so; although they may be removed by washing. Hinds (1982) explains that the adhesive force on a particle less than 10µm is much greater than other forces on such a particle as shown in Table 2-1**.**

Table 2-1 Comparison of adhesive, gravitational, and air current forces on spherical particles of standard density.

	Force (dyn)		
Diameter (µm)	Adhesion [a]	Gravity	Air Current (at 1000 cm/s)
0.1	10^{-3}	5×10^{-13}	2×10^{-5}
1.0	10^{-2}	5×10^{-10}	2×10^{-4}
10	10^{-1}	5×10^{-7}	3×10^{-3}
100	1	5×10^{-4}	6×10^{-2}

[a] Calculated for 50% RH

2.5.4 Re-suspension

Another process closely associated with adhesion of particles is the process of re-suspension. Re-suspension can be defined as the detachment of a particle from a surface and its transport away from the surface. Air jets, mechanical forces, impaction of other particles, or electrostatic forces may result in re-suspension. Re-suspension may involve rolling or sliding of the particle before it becomes airborne.

Wang (1990) describes three different modes of inceptive motions which cause separation. These modes are:

- Lift off - this occurs when the normal component of force acting on an adhered particle exceeds the pull-off force and causes the particle to be lifted off the surface.
- Sliding – during this mode the particle beings to slide and becomes re-suspended. This takes place when the tangential component of an applied force becomes greater than the total normal force (including the sticking force) multiplied by a coefficient of static friction.
- Rolling – this occurs when the total torque about a point on the edge of the contact circle (including the downward sticking force) is equal to zero. This causes the particle to roll around that point and hence off the surface.

Reeks (2001) explains that the action of fluctuating lift and drag couples at the surface of the particle. This leads to a build-up of rotational vibrational energy. Once the adhesive is broken, the particle becomes disconnected from the surface and roles or lifts from the surface (i.e. mechanism of 'incipient rolling' and lift off from the surface). The drag force is the main force in the rolling start off. In fact drag force is almost 100 times greater than the lift force. However, it is the lift force that eventually detaches the particle from the surface.

Re-enterainment is a more specific term used to describe re-suspension by a jet of air. Data from Corn and Stein (1965) for the bulk air velocity required to re-entrain different sizes of glass beads are shown in Figure 2.8. As shown in the figure, the larger the particle and the greater the air velocity, the greater the probability of re-entrainment.

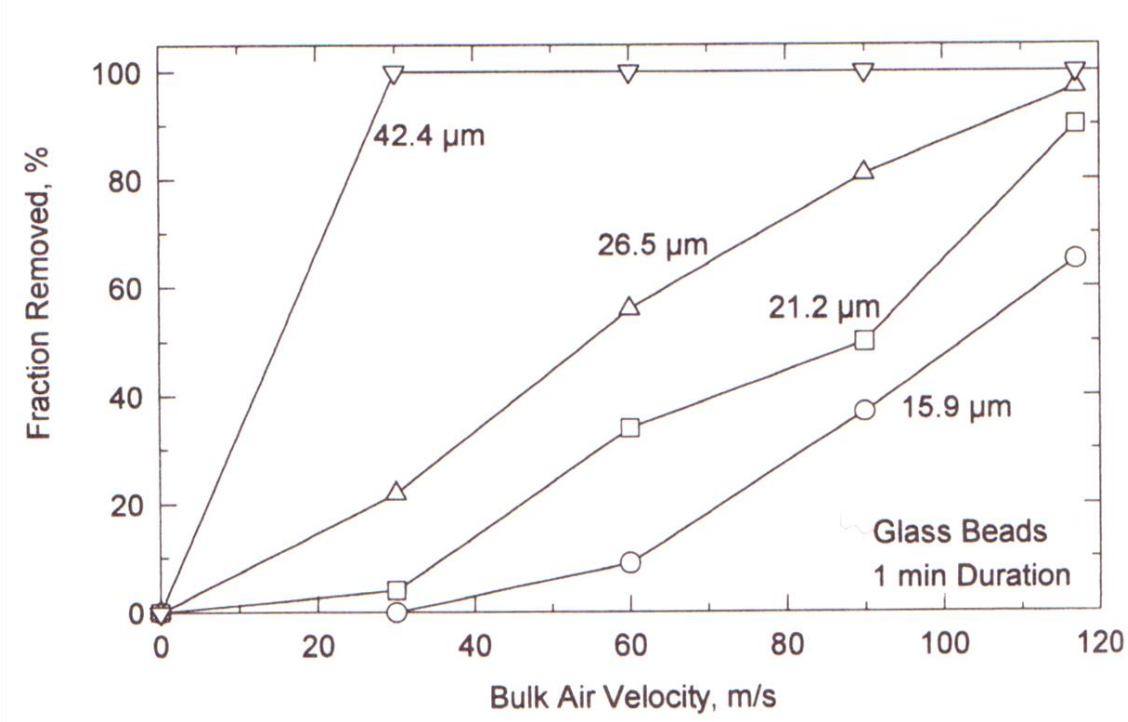

Figure 2.8 - Particle re-entrainment versus bulk air velocity or four particle sizes. Data from Corn and Stein (1965)

Hinds (1982) explains that particles smaller than the boundary layer are in part protected from re-entrainment by being submerged in the boundary layer. Re-entrainment of these particles can be caused by the occasional bursts of turbulent eddies penetrating through the boundary layer.

2.6 Interaction of Light with Suspended Particles

Another factor which needs to be considered in the study of optical windows is the interaction between light and suspended particles. This will be used as the basis of one of the test methods used in this project.

Friedlander (1977) explains that when light hits an aerosol particle, it will either cause scattering or absorption. Scattering refers to when light hits a particle of the same wavelength and the energy received is radiated. The radiation may happen in a different direction with different intensity. Absorption on the other hand, occurs when this energy is transformed into other types of energy such

as heat, chemical reaction, etc. For the purpose of this project scattering is considered.

CHAPTER 3. METHODOLOGY

This chapter explains the thinking and methodology behind the calculations and the experimental work carried out to achieve the results for this project.

In Section 3.1, this chapter begins by providing the details of the hand calculations involved in the design of a new test rig and the reasoning behind the calculations. Section 3.2 introduces the preliminary steps involved in the computational analysis of the new test rig design. Section 3.3 explains the logic behind selecting the window samples for the experiment.

3.1 Calculations

From the review of literature provided in CHAPTER 2. , it is clear that there is not enough information available to obtain conclusive results on the subject of adhesion of particles to optical windows on aircrafts. As a result, an experiment was required. Two main options were considered:

- Completion of a test on the selection of sample windows in an icing tunnel.
- Design of a test rig which provides improved control of the surrounding environment and uses that to perform the relevant tests.

The latter option i.e. utilising a test rig specifically designed for the purpose of this project would provide more control over the variables of the experiments such as flow and air speed, and the introduction of dust particles to the flow. This would generate more exclusive results. The obvious compromise is the time and effort required in the design and construction of the test rig. Both options were considered in this thesis.

3.1.1 Design of the Test Rig

The aim was to design a test rig that demonstrates the behaviour of flow over the side of the aircraft, near the nose of the aircraft. Figure 3.1 depicts the proposed location of the DANIELA windows.

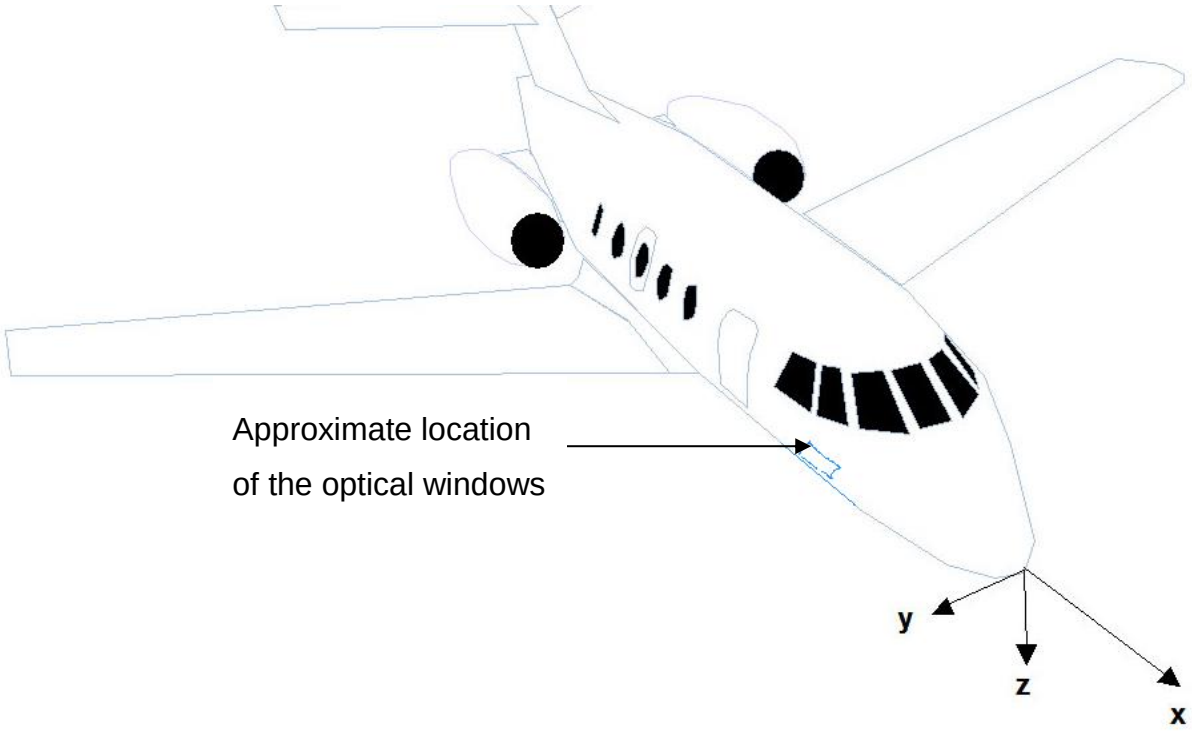

Figure 3.1 Approximate location of the optical windows.

Figure 3.2 demonstrates a schematic of the test rig mechanism. It shows that the air from the lab environment is introduced into the rig from above. It then flows over the bell-mouth and through the rig. Section A-A shows the cross section of the top part of the test which is a hexagonal shape. The rig then becomes cone shaped and the cross section is circular (see Section B-B in Figure 3.2). A fan with a diameter of 0.5 meters is located at the bottom of the rig. As demonstrated in Figure 3.2, the solid particles are fed through the system from above the bell-mouth and are introduced into the system by air flow.

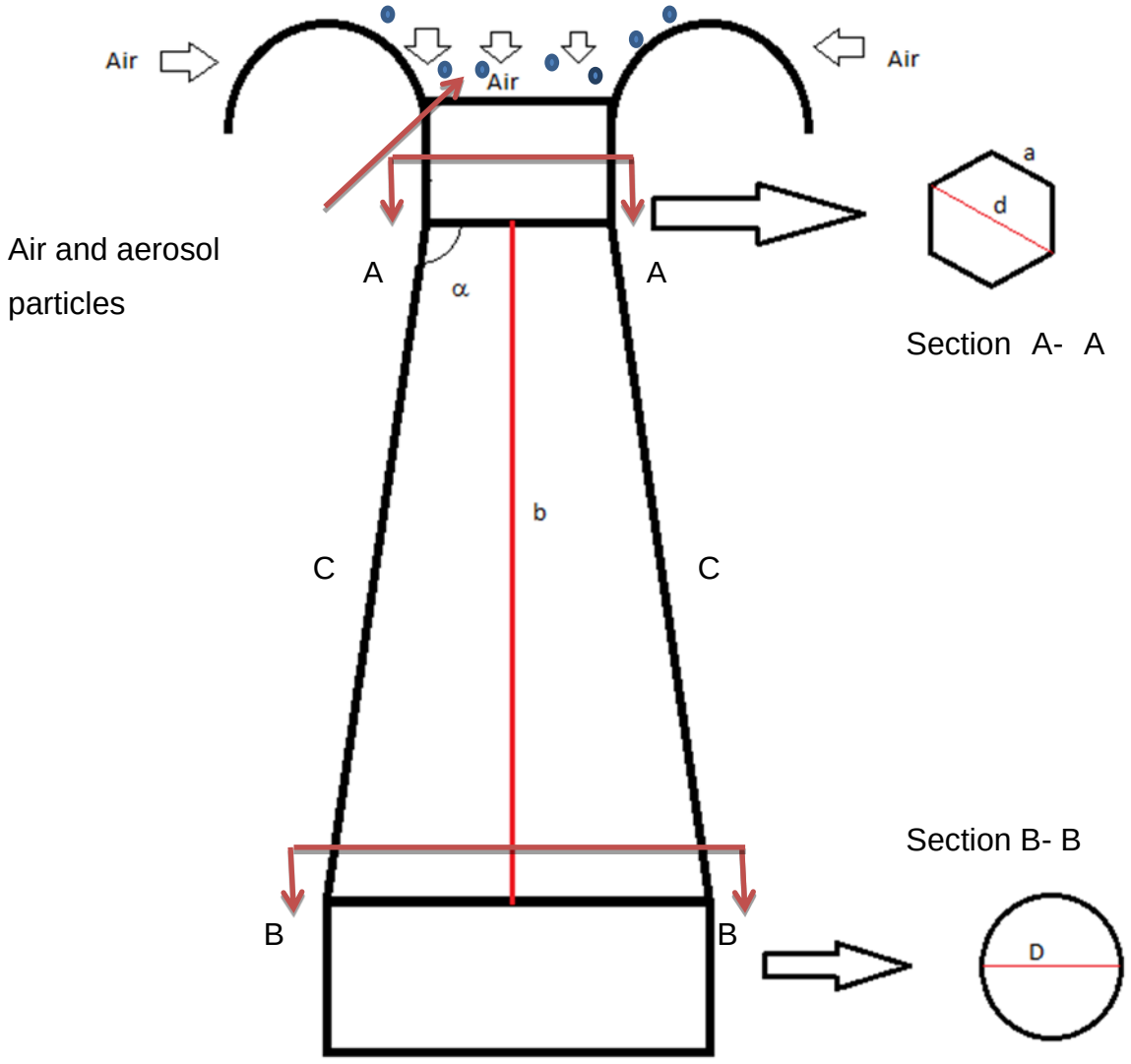

Figure 3.2 Test rig dimensions.

The air speed is 100 m/s which is in the same order of magnitude as the average speed of a civil aircraft. This is a reasonable speed considering the energy consumption and space requirement and the size of the fan required.

To increase the test efficiency, the test was designed to examine the effects of dust particles on 6 different window samples simultaneously. To accommodate this, section A-A (see Figure 3.2) was designed in the shape of a hexagon.

The sample windows have a dimension of 3x5cm. The reason for selecting these dimensions is as follows:

- The samples are not too large to take up too much space and not too small to make them difficult to examine.
- The samples are approximately the same size as microscope slides. This would simplify the study of samples using the microscope.
- The dimension is close to the diameter of DANIELA windows which are 5cm in diameter. Note that the reason for selecting smaller diameter windows for the DANIELA project is that larger windows are more expensive and there is a possibility of manufacturing delays.

The dimension of the side of the hexagon 'a' (see Figure 3.2) was calculated according to the dimension of the window samples to be 0.098m. The area of the hexagon was consequently calculated using

$$A = \frac{3\sqrt{3}}{2} a^2 \quad \textbf{(3-1)}$$

$$A = 0.025 m^2$$

Using A and a, the dimension of the diameter of the hexagon, 'd', (see Figure 3.2) is calculated to be 0.196m.

The volume flow rate can then be calculated according to the flow speed and the inlet area (A), using

$$\dot{V} = V_m \times A \quad \textbf{(3-2)}$$

$$\dot{V} = 2.5 \; {}^{m^3}/_{s} \quad \textbf{(3-3)}$$

The diameter of the fan 'D' (see Figure 3.2) used in this experiment is 0.5 m. The table for the pressure drop and the information on the fan is included in appendix (A).

The angle of expansion from the neck to the diffuser ‘α’ (see Figure 3.2) is 3.5° on each side, as recommended by the manufacturing team.

Next, the vertical length of the middle section of the test rig ‘b’, from the bottom of the hexagon to the top of the fan (see Figure 3.2) can be calculated using Pythagoras theory as

$$X = \frac{D - d}{2} \tag{3-4}$$

and hence

$$b = \frac{X}{\tan \frac{3.5 \times \pi}{180}}$$

$$b = 2.484\ m$$

Therefore, the length of the side edges of the test rig can be calculated as

$$C = \sqrt{L^2 + X^2} \tag{3-5}$$

$$C = 2.488\ m$$

A summary of the test rig parameters is presented in Table 3-1.

Table 3-1 - summary of the test rig parameters

Parameter	Magnitude
Speed in the test rig	100m/s
Size of the windows	0.03 X 0.05m
a (side of the hexagon)	0.098m
Area of the hexagon	0.025m2
Diameter of the hexagon	0.196m
Volume flow rate	2.5m3/s
Diameter of the fan (D)	0.5m
angle of expansion from the neck to the diffuser ‘α’	3.5°
Vertical height of the test rig (b)	2.484m
Side edge length (C)	2.488m

To gain an understanding of the behaviour of the flow in the test rig the Reynolds number is required. Whether a flow is turbulent or laminar is dependent on the geometry, surface roughness, mean fluid velocity, surface temperature, and type of fluid among other things. In fact, the flow regime depends mainly on the ratio of the inertia forces to viscous forces in the fluid which is called the Reynolds number (Čengel and Turner (2001)). For internal flows in circular pipes, the Reynolds number ’Re’ is given by

$$Re = \frac{Inertia\ forces}{Viscous\ Forces} = \frac{V_m D}{v} \quad \textbf{(3-6)}$$

where

V_m = Mean fluid velocity, m/s

D = Characteristic length of the geometry (diameter in this case), m

ν = μ/ρ = Kinematic viscosity of the fluid, m^2/s

μ = Dynamic viscosity

Here, to simplify the calculations, the hexagonal part of the rig is also treated as a circular pipe: Dynamic viscosity of air is 0.0000186kg/m.s and its density is 1.275kg/m^3. Therefore, the Kinematic viscosity of air can be calculated using

$$\nu = \frac{\mu}{\rho} \qquad \textbf{(3-7)}$$

$$\nu = 1.458^{-5}\ {}^{m^2}/_{s}$$

The Reynolds number can then be calculated using equation (3-6) which gives Re = 1.345×10^6.

At large Reynolds numbers inertia forces, which are proportional to density and the velocity of the fluid, are large in comparison to the viscous forces (Čengel and Turner (2001)). Therefore, viscous forces cannot prevent the random and rapid fluctuations of the fluid. On the other hand, at small Reynolds numbers, the viscous forces are large enough to overcome the inertia forces and to keep the fluid “in line”. This results in the flow being turbulent in the first case and laminar in the second.

As Čengel and Turner (2001) point out, having the exact values of Reynolds number for laminar, transitional and turbulent flows is very desirable. However, in practice this is impossible. The reason is that, other factors such as the degree of disturbance of flow by surface roughness, pipe vibrations, and the fluctuations in the flow are also effective on the transition from laminar to turbulent flow. Under most practical conditions, the flow in a pipe is laminar at Re < 2300, turbulent at Re >4000, and transitional in between. That is:

Laminar flow: Re < 2300

Transitional Flow: 2300 ≤ Re ≤ 4000

Turbulent flow: Re > 4000

Therefore, the flow in the test rig across the samples is turbulent, as the previously calculated Reynolds number (1.345×10^6) is much larger than 4000.

To compare this to the Reynolds number on a commercial aircraft, the approximate Reynolds number over the aerofoil of the Airbus A320 was calculated. The Airbus A320 family consists of short to medium range, narrow-body, commercial passenger jet airliners manufactured by Airbus. Airbus A320 is the largest aircraft in this family. The approximate Reynolds number for the Airbus A320 over the aerofoil can be calculated using

$$Re = \frac{Vc}{\nu} \quad \textbf{(3-8)}$$

where

V= Flight speed (m/s)

C = Chord length (m)

ν = Kinematic viscosity (m²/s) = 1.46×10^{-5} (m²/s)

Note that the chord of the aircraft is calculated using

$$C = \frac{s}{b} \quad \textbf{(3-9)}$$

$$C = 3.425\text{m}$$

where

s = Wing area (m²) = 122.6 m²

b = Wing span (m) = 35.80 m

Therefore the chord is 3.425 m and the Reynolds number is calculated to be 5.676×10^7.

Figure 3.4 to Figure 3.6 and Figure 3.8 to Figure 3.10 show the velocity of air versus the position from the nose of the aircraft at 5, 9, 11 and 13m high from the surface of the aircraft. The first set of figures is for a 0˚ side slip condition and the second set is for a 20˚ side slip angle.

The average velocity can be taken as 2.5×10^2 m/s, using which the Reynolds number for the flow within the test rig, can be calculated.

Using equation (3-8), the Reynolds number can then be calculated as:

$$Re = \frac{250 \times 0.196}{1.458^{-5}}$$

Therefore, the Reynolds number for the flow in the test rig, for which the speed of the aircraft is 250 m/s, will be 3.361×10^6.

Figure 3.3 - Figure 3.4 show the velocity profile of the flow around the nose of the aircraft for 0° side slip angle. Figure 3.7 - Figure 3.9, show the velocity vectors at 20° side slip angle on a civil aircraft.

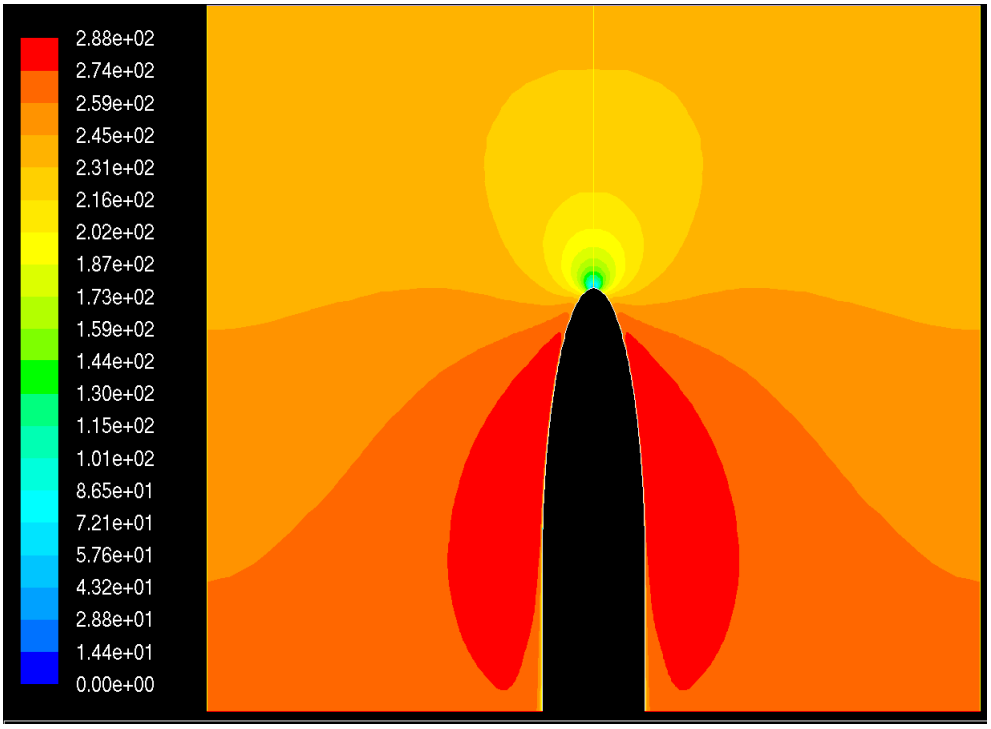

Figure 3.3 Contours of velocity magnitudes for 0° side slip angle.

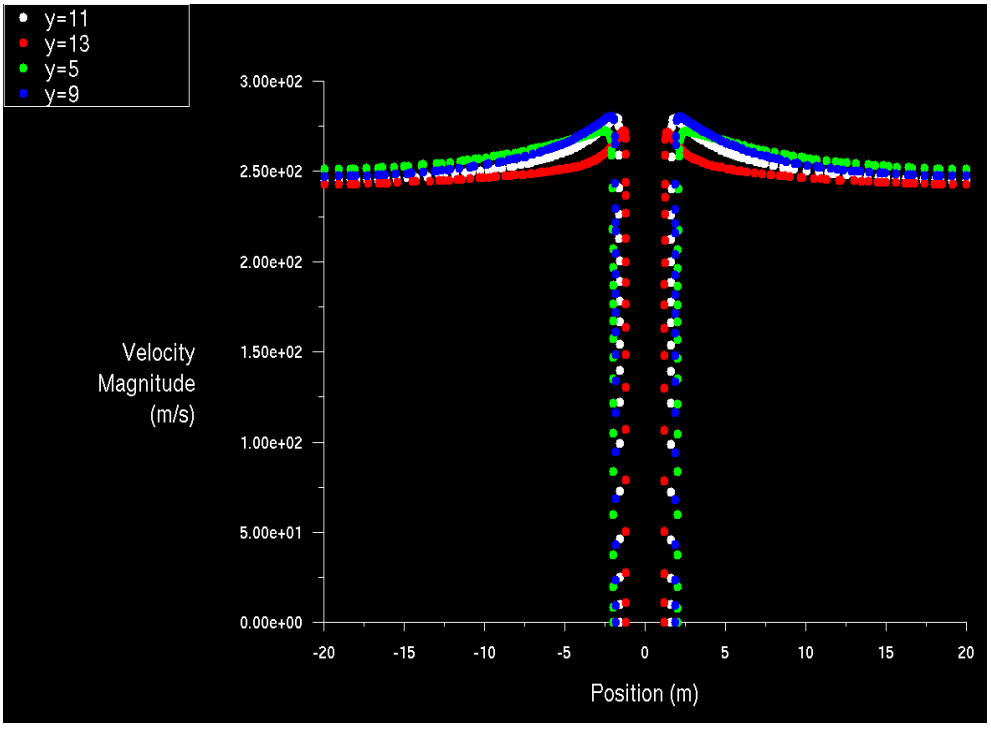

Figure 3.4 Velocity magnitude (m/s) vs position (m) from the nose of the aircraft on both sides.

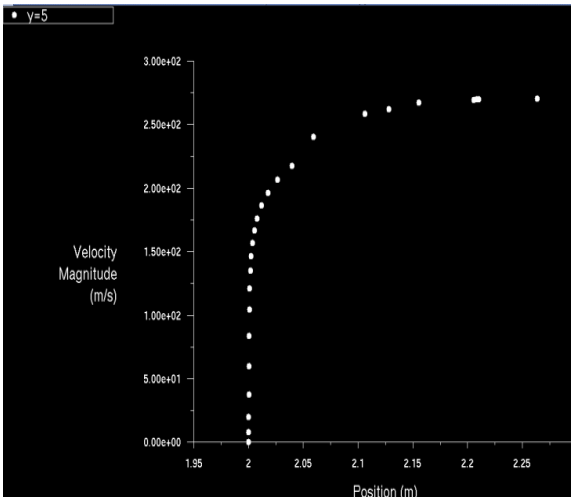

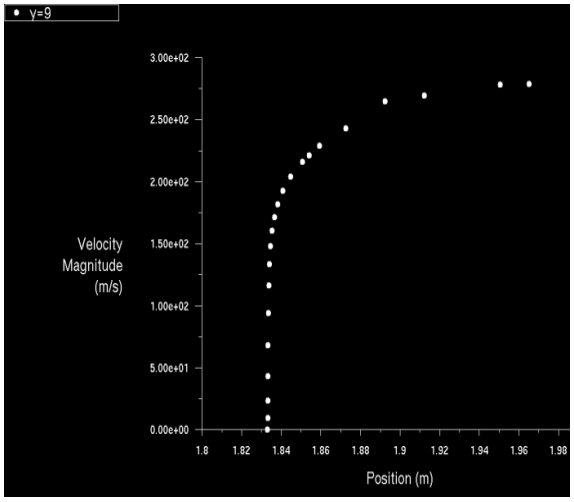

(a) (b)

Figure 3.5 Velocity magnitude (m/s) vs position (m) from the nose of the aircraft at a) a 5m height and b) a 9m height.

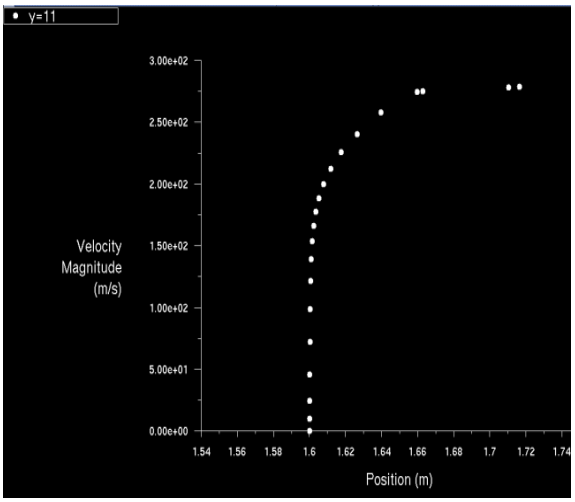

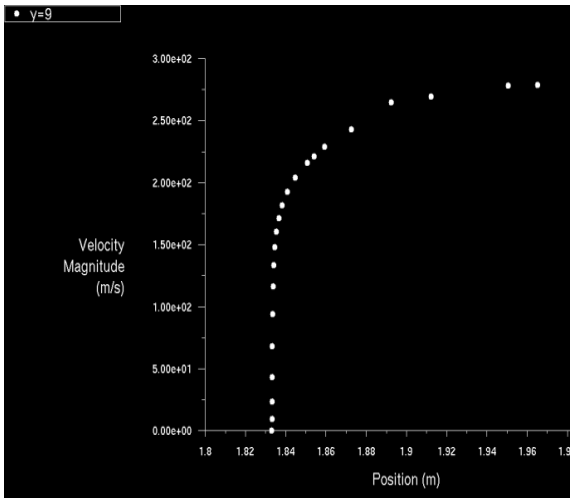

(a) (b)

Figure 3.6 Velocity magnitude (m/s) vs position (m) from the nose of the aircraft at a) a 11m height and b) a 11m height height.

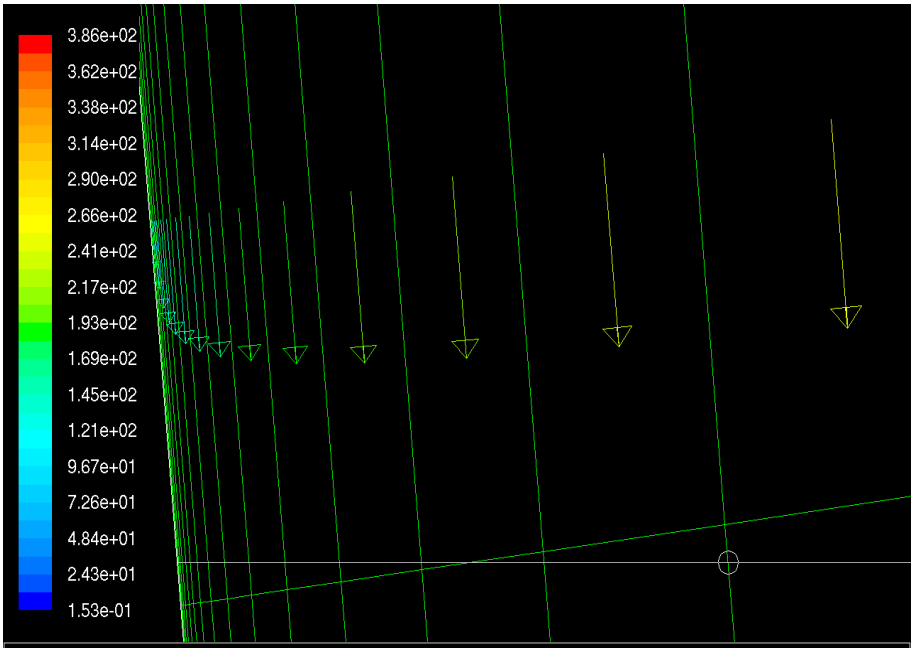

Figure 3.7 Velocity vectors coloured by velocity magnitude (m/s) at 20° side slip angle.

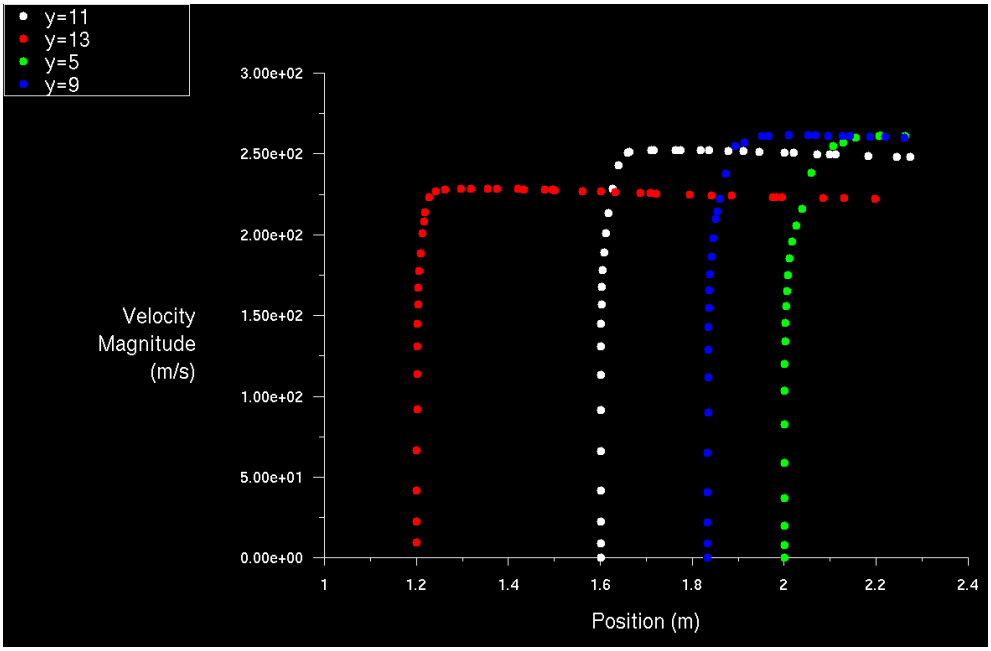

Figure 3.8 Velocity magnitude (m/s) vs distance (m) from the nose of the aircraft at 20° side slip angle.

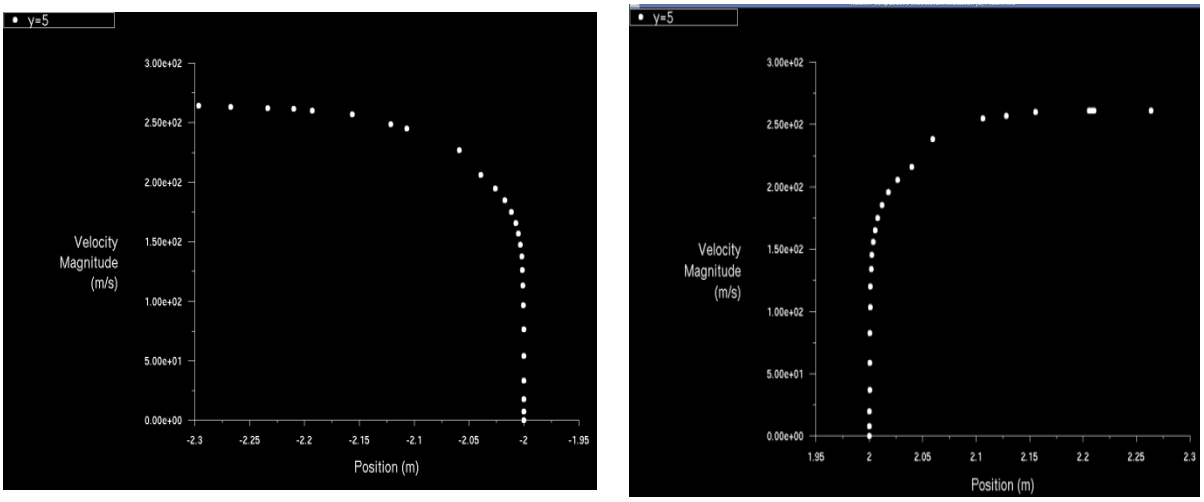

(a) (b)

Figure 3.9 Velocity magnitude (m/s) vs distance (m) from the nose of the aircraft at 5m height at 20° side slip angle – right hand side and b) 13m height at 20° side slip angle.

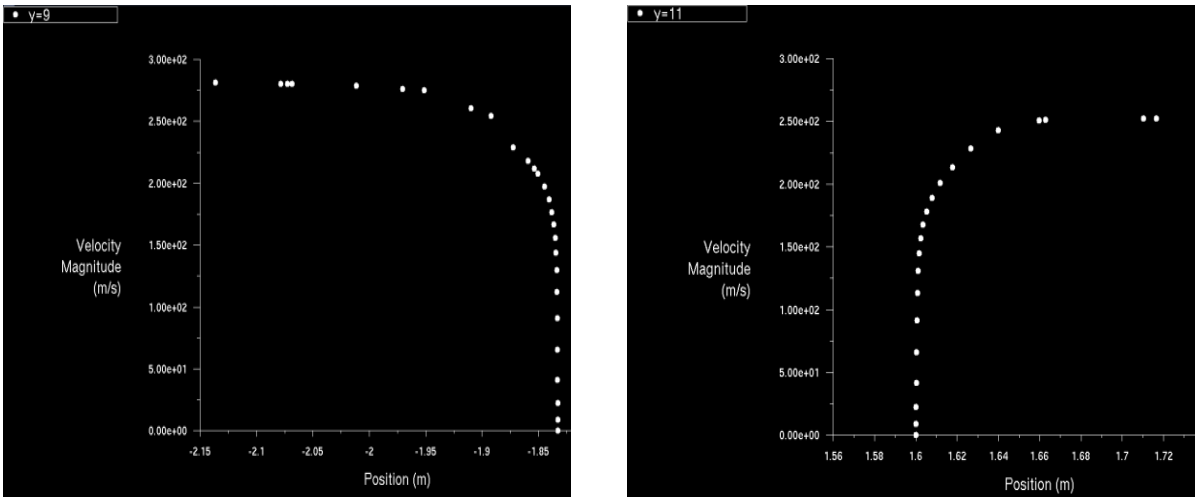

(a) **(b)**

Figure 3.10 Velocity magnitude (m/s) vs distance (m) from the nose of the aircraft at a) 9cm height at 20° side slip angle and b) 5cm height at 20° side slip angle.

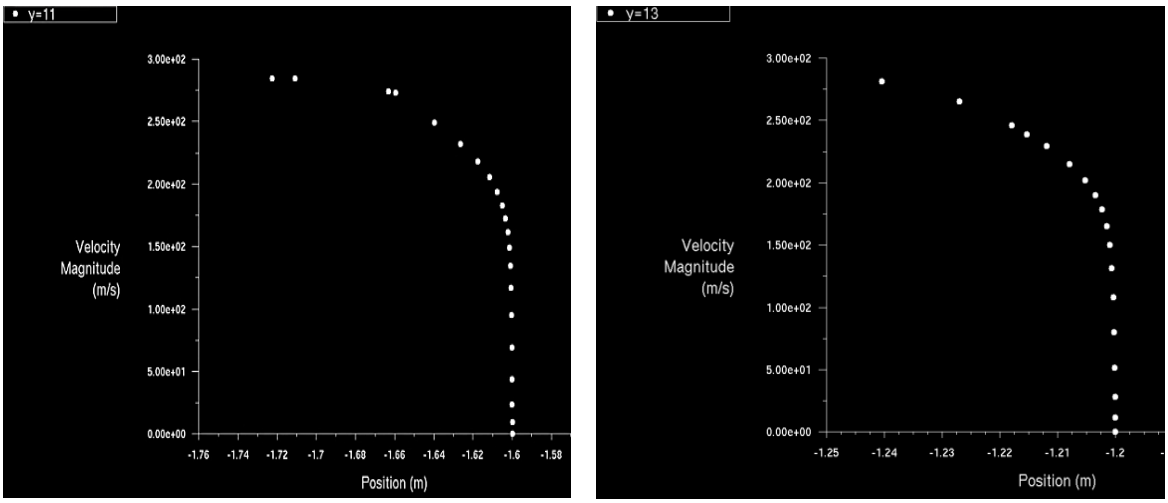

(a) (b)

Figure 3.11 Velocity magnitude (m/s) vs distance (m) from the nose of the aircraft at 5m height at 20° side slip angle – left hand side and b) 13m height at 20° side slip angle.

Figure 3.9 – Figure 3.11 show the change in velocity versus the distance from the surface of the aircraft at y= 5, 9, 11 and 13 m which is the distance from the nose of the aircraft along the fuselage. It can be seen that the velocity increases from zero (at x = 2m) to approximately 80% of the highest value shown on these figures at x = 2.05 m.

Table 3-2 exhibits the Reynolds numbers achieved from different calculations explained above. The values achieved from Adair Williams calculations proves that the flow over the nose of the air craft is a turbulent flow and this can be achieved within the test rig. Therefore not only the velocity within the test rig is of the same order of magnitude as a civil air craft, the flow is also turbulent. This shows that the test will create a better demonstration of the behaviour of flow over the DANIELA windows.

Table 3-2 Reynolds numbers obtained under different conditions.

Method	Reynolds Number
Test rig	1.345×10^6
Commercial air craft	5.676×10^7
Adair William's calculations	3.361×10^6

Another value which needs to be considered is the boundary layer thickness. To achieve this, the windows have to be placed at a certain distance from the rig inlet. To reach the desirable distance, investigations are required to determine the boundary layer thickness and entry length.

To explain the inlet region and entry length, Čengel and Turner (2001) considered a fluid entering a circular pipe with uniform velocity. Due to non-slip conditions, the particles in the layer in contact with the surface of the pipe will come to a complete stop. Consequently, the neighbouring fluid layer will slow down as a result of friction between the particles of these two adjoining fluid layers at different velocities. This fluid layer will then slow down the molecules of the next layer, and so on. To make up for the velocity reduction in flow and to maintain a constant mass flow rate through the pipe, the velocity at the mid-section of the pipe has to increase. This will result in a velocity gradient developing along the pipe.

The boundary layer is a region of the flow in which the effects of the viscous shearing force caused by fluid viscosity are felt. The hypothetical boundary surface divides the flow in the cross section of the pipe into two regions: the boundary layer region, in which the viscous effects and the velocity changes are significant, and the inviscid flow region, in which frictional effects are negligible and the velocity remains essentially constant.

The boundary layer thickness increases in the direction of the flow until the boundary layer reaches the centre of the pipe and therefore fills the centre of the pipe. Čengel and turner (2001) refer to the region from the pipe inlet to the

point where the boundary layer merges as the *hydrodynamic entry region entrance length* L_h or the *entrance length*. The hydro-dynamically developed region is referred to as the region beyond the hydrodynamic entry area in which the velocity profile is fully developed and remains unchanged. Fully developed flow occurs when the normalised temperature profile also remains constant. When the fluid temperature does not vary in the pipe and stays constant throughout, the hydro-dynamically developed flow is equivalent to the fully developed flow. The profile of mean velocity in hydro-dynamically developed regions is parabolic in laminar flows and flatter in turbulent flows. The hydrodynamic entry length in laminar flow in a pipe is given approximately by

$$L_{h,laminar} \approx 0.06\, ReD \tag{3-10}$$

In turbulent flow, the intense mixing during random fluctuations usually overshadows the effects of momentum diffusion. For smooth pipes, the hydrodynamic entry length is expressed as:

$$L_{h,Turbulent} \approx 4.4\, D\, (Re)^{1/6} \tag{3-11}$$

Hence, the entry length for the test rig is evaluated as

$$L_{h,Turbulent} \approx 4.4 \times 0.196 \times (1.345 \times 10^{6})^{1/6} \tag{3-12}$$

$$\approx 9.069\, m$$

A boundary layer thickness of one centimetre is selected. This boundary layer had been previously calculated and used by Adiar Williams as part of the DANIELA project.

3.1.2 Pressure Loss in the Test Rig

Another factor that required consideration was the pressure drop through the test rig, to ensure that there will be adequate pressure to move the particles through the rig.

Čengel and Turner (2001) express the pressure drop as a result of friction effects for internal flows as

$$\Delta P = f\frac{L}{D}\frac{\rho V_m^2}{2} \tag{3-13}$$

where $\rho {V_m^2}/{2}$ is the dynamic pressure. The dimensionless quantity f is the friction factor. For a fully laminar flow the friction factor can be expressed as

$$f = \frac{64\mu}{\rho D V_m} = \frac{64}{Re} \tag{3-14}$$

Whilst for fully turbulent flows, such as the flow in the test rig, the friction factor can be calculated using

$$\frac{1}{\sqrt{f}} \approx -1.8log\left[\frac{6.9}{Re} + \left(\frac{{\varepsilon}/{D}}{3.7}\right)^{1.11}\right] \tag{3-15}$$

The head loss is defined by

$$h_l = \frac{\Delta P}{\rho g} = f\frac{L}{D}\frac{V_m^2}{2g} \tag{3-16}$$

However, for minor losses in the system, h_l can be calculated using

$$h_l = K_L\frac{V_m^2}{2g} \tag{3-17}$$

where K_L is the loss coefficient.

To calculate the pressure drop across the test rig, the rig was divided into three sections: the neck area, the diffuser and the main part. However, note that minor head losses occur in the bell-mouth and also in the expansion of the neck to the diffuser.

To calculate the head loss at the entrance to the rig, the bell-mouth is assumed to be well rounded. Using the head loss coefficients from Čengel and Turner (2001), the ratio of the radius of the bell-mouth to the diameter of the test rig at

the neck area is assumed to be equal to 0.2. This will prove a value of 0.039 for the radius of the bell-mouth.

The head loss can then be calculated to be 15.29m using equation (3-17).

Rearranging equation (3-16) to calculate pressure drop gives

$$\Delta p = h_l \rho g \quad \textbf{(3-18)}$$

This gives the pressure drop in the entrance to be 187.5 Pa. The pressure drop at the neck area of the test rig is due to the friction losses at this area.

To calculate the pressure drop, equation (3-16) is used to calculate the friction loss and the result is placed in equation (3-17) to arrive at the pressure drop value of 318.6 Pa.

To calculate the head loss in the expansion of the pipe, the expansion angle is assumed to be 8°. This gives a head loss coefficient of 0.02 as explained by Čengel and Turner (2001). Using equation (3-17), the head loss is calculated to be 10.19m and the pressure drop is then calculated using equation (3-18) to be 25.3Pa.

Therefore, the total pressure drop throughout the test rig is approximately equal to the sum of all the pressure drops calculated, which is 531.4Pa.

Table 3-3 shows the pressure drop calculated in the different sections of the test rig.

Table 3-3 Pressure drop calculated in different sections of the test rig.

Location	Pressure
At the entrance of the test rig	187.5 Pa
At the neck of the test rig	318.6 Pa
Expansion section of the test rig	25.3Pa
Overall pressure drop in the test rig	531.4Pa

Using the above results, a suitable fan can be selected which is able to overcome the pressure drop in the system.

3.1.3 Boundary Layer Thickness

To define the boundary layer thickness of the flow, some arbitrary convention must be adapted as the velocity within the boundary layer approaches the velocity of the main stream asymptotically. One way of describing the thickness is the distance from the solid surface at which the velocity reaches 99% of maximum velocity U_m of the main stream. To increase the chance of the window samples being affected by the dust particles as they would be on an aircraft, a boundary layer thickness of 1cm was chosen.

In order to collect the dust particles after they leave the rig a pack of filters needs to be placed between the fan and the rig.

The test can be undertaken with just air from atmosphere going through the test rig. However this can be further expanded by using vegetable oil as an example of droplets and “Arizona dust” (ISO 12103 Ptl –Grade A1) as solid particles.

3.1.4 Discharge Coefficient

Another factor which needs to be considered in designing the test rig, which could affect the flow and the boundary layer thickness, is the discharge coefficient. Blaire et al describe that the shape of the bell-mouth at the intake can play an important part on the characteristics of the flow. Hence further investigation was completed on studying the flow over the bell mouth on ICEM Computational Fluid Dynamics (CFD), to ensure that a suitable flow is built in the rig and that a reasonable boundary layer thickness of around 1cm is built up over the window samples. This is explained fully in 3.2. Massey (2006) explains that as a result of friction and contraction, the discharge from the orifice is less than the ideal value and the coefficient of discharge C_d is defined as the ratio of the actual discharge to the ideal value i.e.

$$C_d = \frac{Actual\ discharge}{Ideal\ discharge} \qquad \textbf{(3-19)}$$

$$= \frac{\boldsymbol{Area\ of\ vena\ contracta \times Actual\ velocity\ there}}{\boldsymbol{Ideal\ cross\ sectional\ area \times Ideal\ velocity}}$$

$$= \frac{Area\ of\ vena\ contracta\ \times Actual\ velocity}{Area\ of\ orifice\ \times Ideal\ velocity} = C_c \times C_v$$

3.2 Computational Fluid Dynamics Work

In order to determine the behaviour of the flow over the window samples and along the test rig, a numerical modelling and simulation work was carried out in the CFD module of the software package ANSYS.

Figure 3.12 depicts the geometry and the mesh of the test rig, which was created in ICEM. As shown in this figure, the test rig is divided into two equal parts. Only half of the test rig is modelled and using axis symmetry, the whole test rig can then be studied. Once the geometry is created, the model is discretised into finite control volumes. The close up of the resulting mesh near the bell mouth and the test rig inlet is demonstrated in Figure 3.13.

After the geometry and a mesh were created in ICEM, they were imported to the CFD solver FLUENT to be processed.

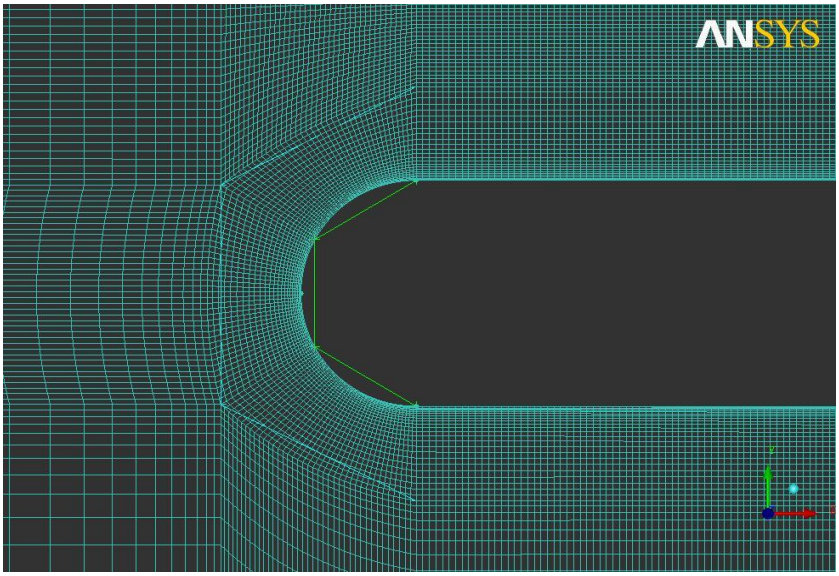

Figure 3.12 Geometry of the test rig in ICEM

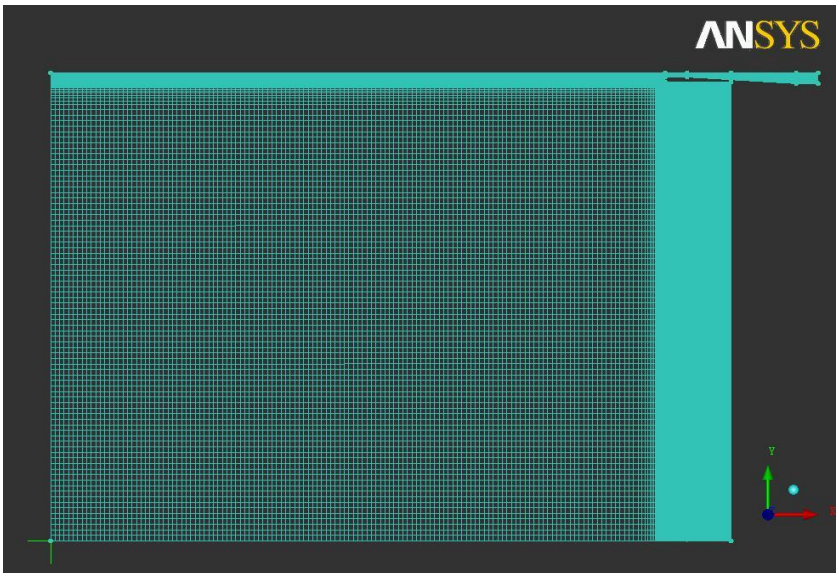

Figure 3.13 The entrance of the test rig.

3.2.1 Fluent Work and Results

As Jiyuan Tu et al (2007) explains, to be able to study the behaviour of the flow in a test rig, the fluid properties need to be understood and defined in Fluent.

As the flow inside and outside the test rig needs to be studied, both internal and external flows need to be considered. As mentioned before, to start with, the fluid flowing through the icing tunnel is air, which is considered to be inviscid and incompressible. The materials properties of air are used in FLUENT accordingly.

Once the properties of air are defined, the boundary conditions are assigned. Figure 3.14 illustrates the implemented boundary conditions. The line at the top of the sketch is the pressure inlet at which pressure is set to atmospheric pressure i.e. 101325 Pa and velocity is set to the inlet velocity i.e. 100 m/s. The far left line is the wall of the laboratory in which the rig is placed. The lower line next to the wall is a pressure inlet. The blue line shows the body of the rig which

is denoted by wall 2. The fan outlet is defined as an outlet. Finally, symmetry boundary conditions are applied at the axis of symmetry of the half model.

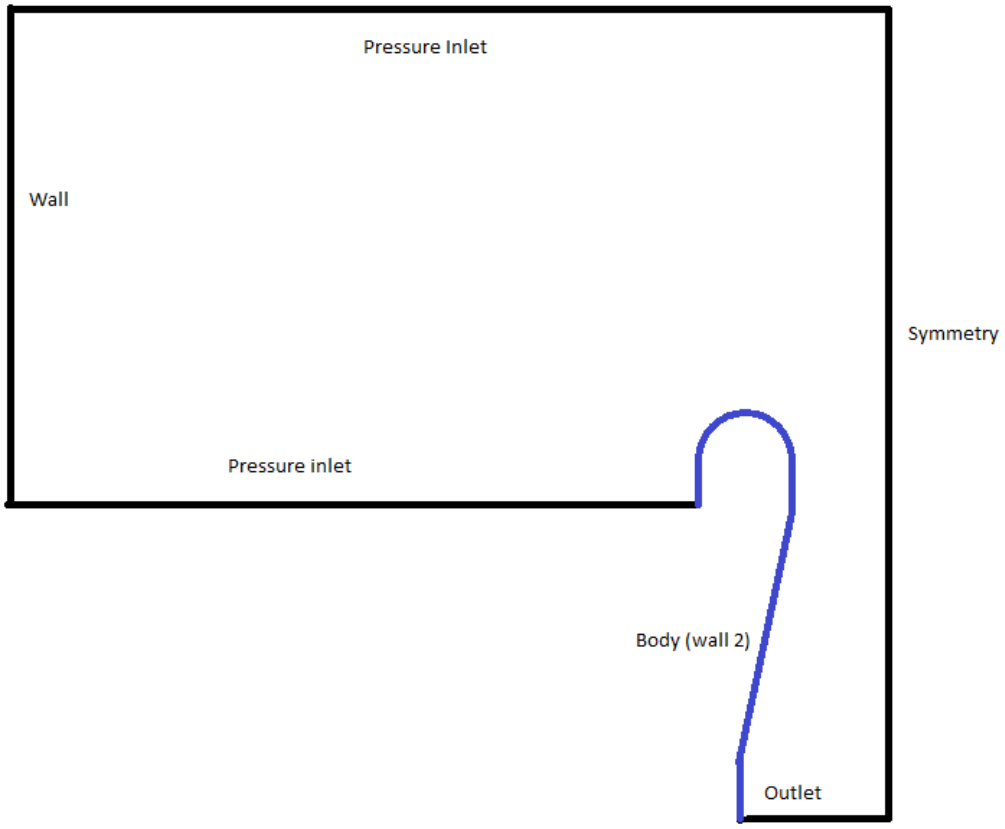

Figure 3.14 Boundary Conditions.

The analysis completed shows that, considering the given parameters, the flow can be achieved within the test rig.

3.3 Windows Samples

There are a number of factors which could affect the selection of the windows. Some of these factors are the forces between the surface of the optical window and the aerosol particles. These forces are the adhesive forces, which include:

- Van der Waals force
- Electro-static Force
- Forces arising from the surface tension of absorb liquid films.

In addition to the forces acting between the aerosol particles and the surface, there are other qualities that the windows should possess for the purpose of this project. These include optical properties, mechanical properties, thermal properties and the way the materials have been manufactured. Additionally, different ways exist in obtaining what is needed from an optical window in terms of resistance and strength by applying different type of coating to these materials.

There are different methods to measure the resistance of various materials to erosion, including using high speed water jet bursts produced by multiple impact jet apparatus (MIJA) developed by Cambridge University. (DANIELA 6 monthly report – 2008)

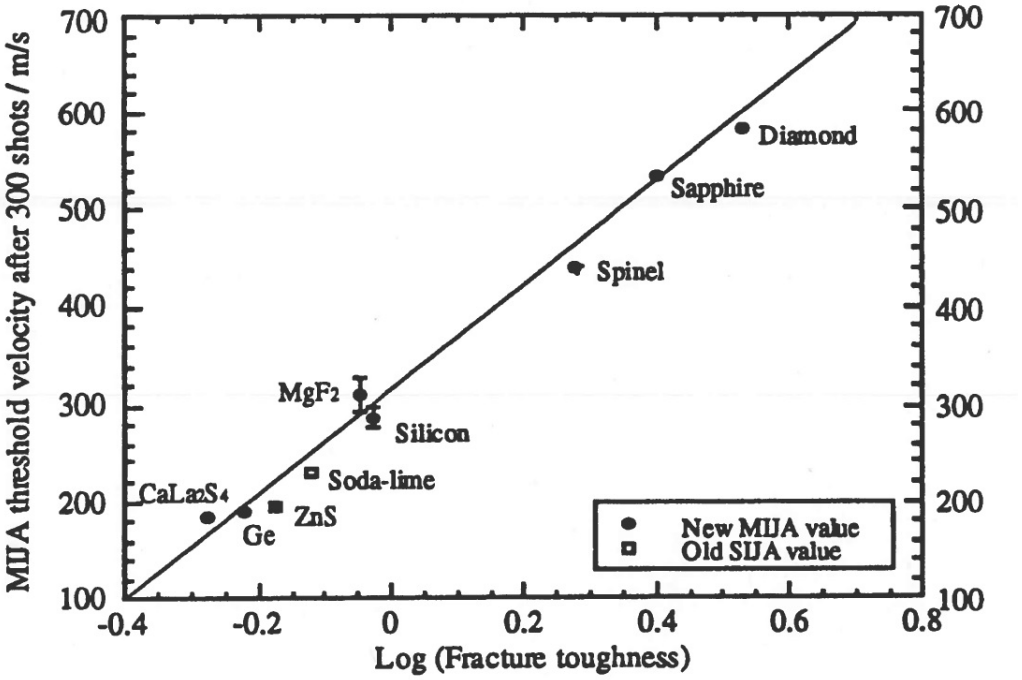

Figure 3.15 Summary of damage threshold for a range of window materials for normal incidents subject to water jet impact 1994.

Figure 3.15 shows a strong link between the jet impact speed at which a material surface shows some permanent damage and the fracture toughness of that material. The jet is thought to have a similar impact to that of a water droplet of 2mm diameter acting at a similar speed in normal impact.

Harris (1999) divides bulk infrared window materials into three different groups: crystals, polycrystalline and glasses. Table 3-4 shows some of the examples of each group.

Table 3-4 Classes of bulk infrared materials.

Class of material	Examples
Single-crystal	Sapphire (Al_2O_3), Si, Ge, GaAs, CaF_2, LiF, KBr, NaCl
Polycrystalline	Hot pressed: MgF_2 and other Irtran®* materials Hot isostatically pressed: Y_2O_3 Hot pressed and hot isostatically pressed: Spinel ($MgAl_2O_4$) Sintered: ALON ($9Al_2O_3 \cdot 5AlN$), lanthana-doped yttria Chemical vapor deposited: ZnS, ZnSe, diamond, Si, SiC Melt growth with cm-size grains: Si, Ge, GaAs, GaP
Glass	Midwave materials (3-5 μm) Calcium aluminate ($43\%CaO\text{-}47\%Al_2O_3\text{-}10\%BaO$) Germanate ($33\%GeO_2\text{-}37\%Al_2O_3\text{-}20\%CaO\text{-}5\%BaO\text{-}5\%$ ZnO) Fluoride[1] ($ZrF_4/HfF_4/BaF_2$) Fused silica (SiO_2) Long wave materials[2] (8-12 μm) Chalcogenides (S, Se, Te + other elements) AMTIR-1®† ($Ge_{33}As_{12}Se_{55}$) Arsenic trisulfide[3] (As_2S_3) Chalcogenide halide[4] ($Te_2Se_3IAs_4$)

*Irtran is a trademark for materials formerly manufactured by Eastman Kodak. The compositions are Irtran 1 = MgF_2, Irtran 2, = ZnS, Irtran 3 = CaF_2, Irtran 4 = ZnSe, Irtran 5 = MgO and Irtran 6 = CdTe.

†AMTIR is a trademark of Amorphous Materials, Inc.

Harris (1999) also describes how in crystal materials all the atoms are aligned regularly. Throughout the crystal, the arrangement of atoms within each cell unit is identical.

In glass materials, there is no regularity or crystalline form. The connection from one cell to another twists and turns. Therefore, the structure does not repeat itself from one region to another.

A polycrystalline material is made up of randomly oriented crystals called grains. The grain boundaries are holding the material together; as a result the thickness. The composition of the grain boundaries is very effective on the strength of the material. The grain boundaries can also affect the thermal conductivity of the material, as the heat does not flow across boundaries at the same rate. (Harris - 1999)

It is also explained by Harris (1999) that the polycrystalline materials are usually cheaper, and tend to be tougher and stronger than single crystals of the same material. Glass materials are easier to fabricate. They can be manufactured in large shapes with good optical qualities. However, the downside to glasses is the lower mechanical properties, which makes them less durable.

CHAPTER 4. EXPERIMENTAL WORK

As mentioned previously two experimental approaches are possible:

1) Experiments using an existing icing tunnel,

2) Experiments using a newly designed test rig for the purpose of this project. Both methods were considered in this thesis.

As explained in Section 3.1.1, the design of the new test rig was completed. However, the test rig construction required more time and resources, which did not become available prior to the termination of the project. Nonetheless, the theoretical work presented in Section 3.1 can be utilised in the building of the test rig in the future in order to perform more specific tests under more controlled conditions. The experimental procedure carried out by placing the window samples inside an existing icing tunnel is described in this chapter.

This chapter starts by introducing the tools required for the experiment in Section 4.1. It then outlines the objective of the experiment in Section 4.2 before describing the experiment procedures in Section 4.3.

4.1 Tools Required

For the purpose of the experiment a metal frame was manufactured with 6 slots for the samples and these were then placed in Cranfield icing tunnel.

4.1.1 Window Samples and Frame:

Six window samples of sizes 3x5cm were fixed in an aluminium frame and attached to the surface of the top wall of the icing tunnel as shown in Figure 4.1 and Figure 4.2.

To be able to test the effect of particle adhesion on all classes of the materials described in section 3.3, one or two samples of each class was selected. The following materials were purchased to be tested:

- Sapphire (Single crystal)
- Germanium (Single crystal)

- BK7 (Glass)
- Zinc Sulphite (Polycrystalline)

Sapphire

Sapphire which is a single crystal aluminium oxide (α-Al_2O_3) is one of the popular infrared materials used for windows which survive in challenging environments (Harris - 1999).

Germanium

According to Sullivan (2009), Germanium is transparent in both long wave (8-12μm) and short wave (3-5μm). However, according to Avsar et al (2010) to increase the windows strength and durability, a coating of Diamond-Like Carbon (DLC), is deposited on the germanium.

BK7 (Crown glass)

BK7 is a borosilicate crown optical glass. BK7 has a high homogeneity and low bubble content. Albeit glasses are easier to manufacture and can be produced in large shapes with good optical quality, they suffer from inferior mechanical properties compared to the other two classes of materials.

Zinc Sulphide (ZnS) – Chemical Vapour Deposition (CVD)

Chemical Vapour Deposition (CVD) is a process of passing gaseous reactants over a hot substrate. The gaseous reactants are hence decomposed and produce a solid material as explained by Kaplan et al (1998). The CVD optical materials are polycrystalline. Zinc sulphite however is weak against erosion and requires a protective coating.

The above materials all possess the optical quality and are resistant to most environments or can be made resistant with coatings.

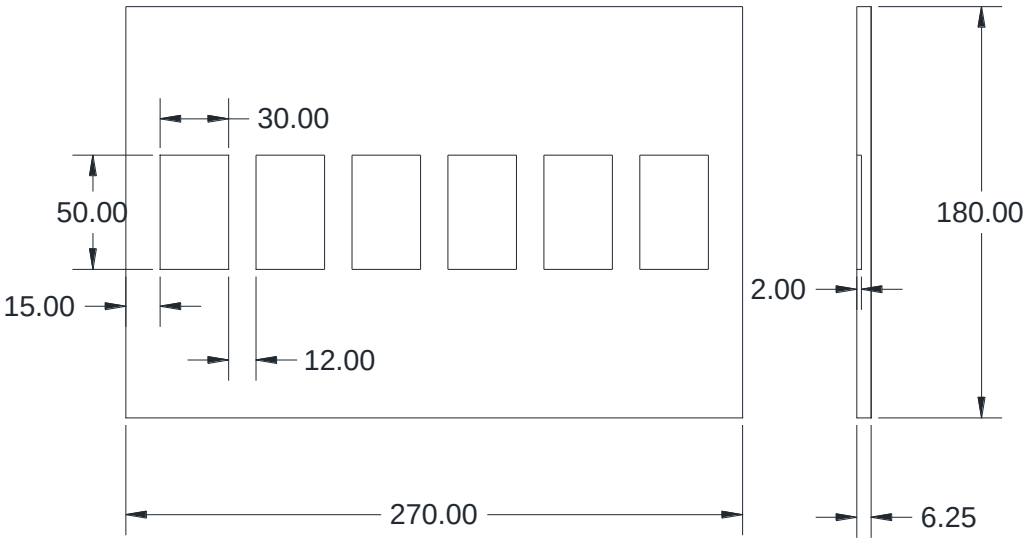

Figure 4.1 Window samples' frame dimensions.

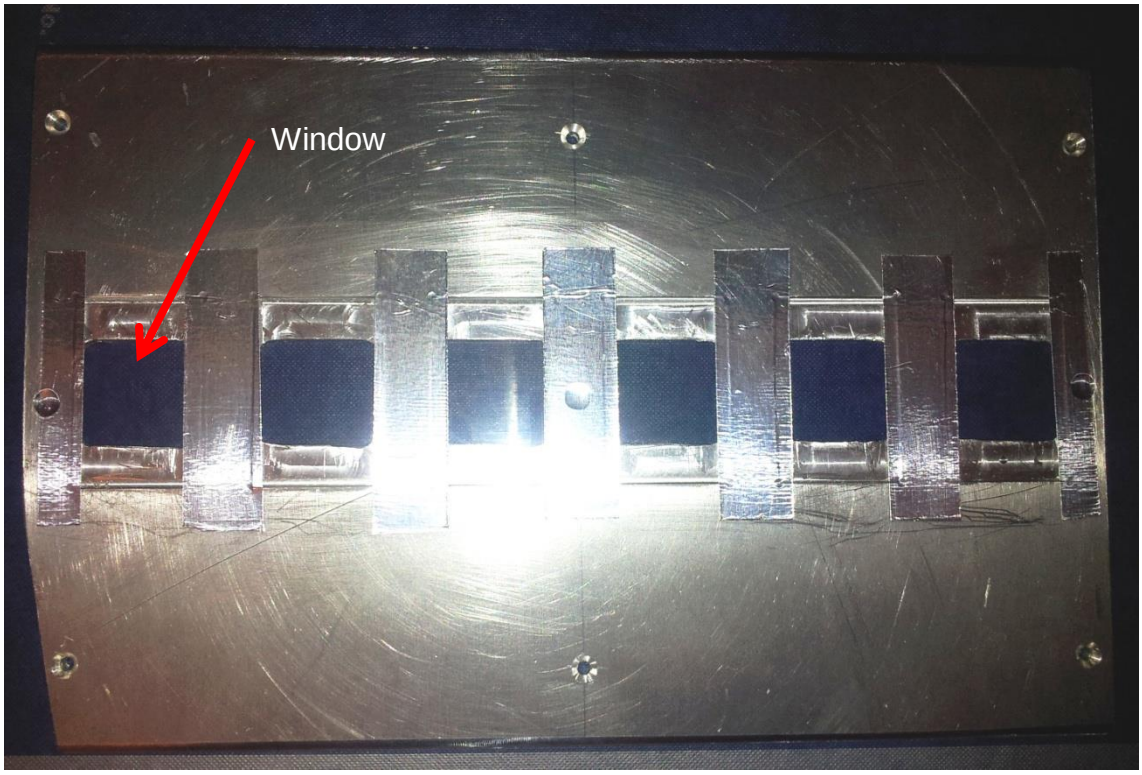

Figure 4.2 Samples in the metal frame.

4.1.2 Icing Tunnel:

Icing tunnels are generally similar to standard aerodynamic wind tunnels. However the main difference between an icing tunnel and a wind tunnel is the addition of a refrigeration plant, to cool the airflow at a range of temperatures between 0 and -35 degree and to include a droplet source of bar spray rake with nozzles able to produce droplet sizes. (Sorato – 2009)

Cranfield Icing tunnel contains an 80 Kg/s fan with a series of different working sections which allows obtaining a test mach number from 0.1 to 0.5. The atmospheric icing conditions are simulated with a refrigeration plant with a cooler of 450 KW able to decrease the temperature from 30°C to -30°C. With six spray bars of nozzles, the icing tunnel is able to produce droplet sizes from 15 to 80 micron. The tunnel is equipped with several pressure and temperature transducers which are fixed and connected to the digital data acquisition system and used to monitor and control the tunnel running conditions. (Cranfield University Website – 2016)

The icing tunnel consists of the following sections: test section, divergent section, turning vanes, plenum chamber and convergent section. Figure 4.3 demonstrates a section view of the icing tunnel. (Sorato – 2009)

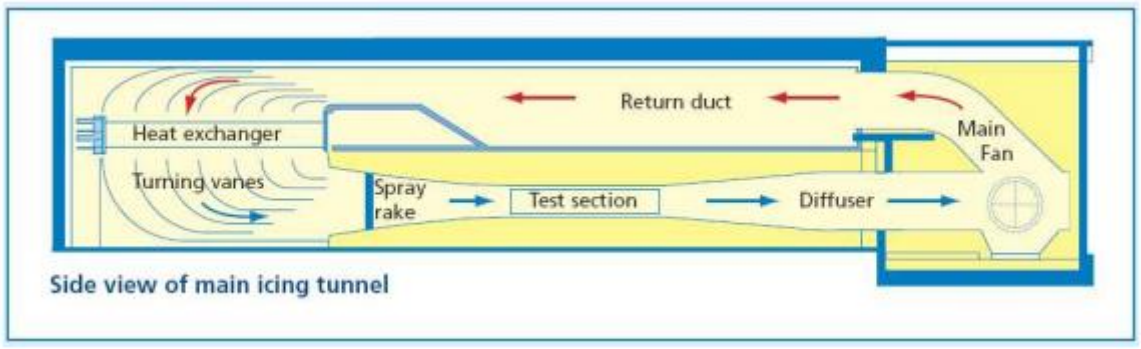

Figure 4.3 – Cranfield icing wind tunnel view (Cranfield University Website – 2016)

The frame containing the window samples was attached to the upper wall within the test section of the icing tunnel.

To study the flow profile within the icing tunnel, at the location where the samples were to be tested, pressure measurements were obtained using a Pitot tube. The flow velocity was then calculated using the Bernoulli equation expressed as

$$P_1 - P_2 = {}^1/_2\,\rho(V_2^2 - V_1^2) \quad \textbf{(4-1)}$$

where the air speed, pressure and density are

Air Speed (V_1): 50m/s

Air pressure (P_1): 24000 Pa

Air density at -10° C (ρ): 1.25347kg/m3

P_2 is the pressure measured using the pitot tube at different vertical distances from the wall of the icing tunnel at the location of the samples. To improve the accuracy, three sets of measurements were taken for each point and the average was calculated as shown in Table 4-1.

Equation (4-1) can then be rearranged to calculate the flow velocity at different vertical distances from the icing tunnel wall, at the location of the samples.

$$V_2 = \sqrt{\frac{2 \times (P_1 - P_2)}{\rho} + V_1^2} \quad \textbf{(4-2)}$$

The calculated velocity is presented in Table 4-1. Figure 4.4 demonstrates the flow velocity profile of the icing tunnel.

Table 4-1 Pressure reading and velocity profile at different distance from the wall of the icing tunnel.

Distance from wall	Reading 1	Reading 2	Reading 3	Average Reading	Velocity
mm	Pa	Pa	Pa	Pa	m/s
2	839	828	862	843	37.35
3	840	852	866	853	37.56
4	900	911	902	904	38.64
5	921	933	903	919	38.94
6	933	956	944	944	39.46
10	975	984	992	984	40.24
20	1007	1024	1015	1015	40.87
30	1009	1041	1015	1022	40.99
40	1015	1023	1001	1013	40.82

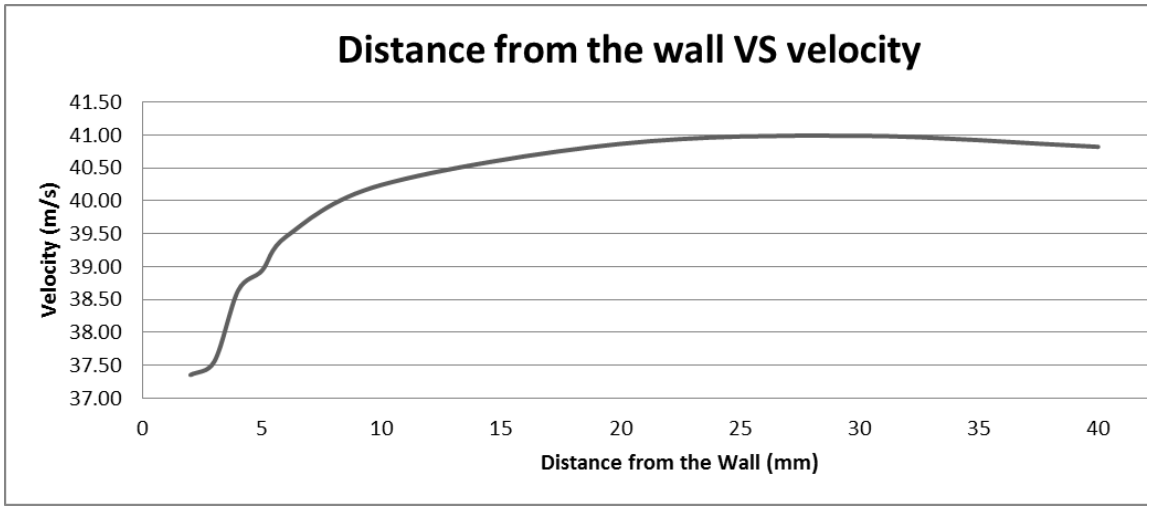

Figure 4.4 - Icing tunnel flow velocity against distance from the wall of the icing tunnel.

The frame in which the samples are placed has a thickness of 6.25mm. The flow velocity near the surface of the samples is therefore approximately 39.5m/s.

4.1.3 Optical Testing Station

An optical testing station was manufactured to test the optical clarity of the window samples. This station included an optical device and a sensor.

Prior to the built up of the optical station, a prototype of the optical station was created to test the hypothesis of the effectiveness of measuring the amount of back scatter from the windows. The prototype proved effective, and hence an optical station was created for the purpose of this experiment.

The concept behind the optical set up is as shown in Figure 4.5.

Figure 4.5 Optical test station.

$$V_r + V_d = V_s \quad \textbf{(4-3)}$$

where,

V_r = Voltage across the resistor (is the value being considered for comparison)

V_d = Voltage across the diode

V_s = Voltage across the battery

The optical station consisted of a 635 nm laser diode module set at 2.6V, a SI pin photodiode with a sensitivity of 320 to 1100 nm and a fixed frame which the samples were placed in. The reason for selecting the specific laser diode was the visibility of the light signal which eased the testing.

The laser was placed at 45° angle to the samples at 7cm distance and the diode was placed directly at a 90° angle in front of the samples at 2cm distance. This was to prevent the sensor picking up the reflection from the samples. This is demonstrated in Figure 4.6.

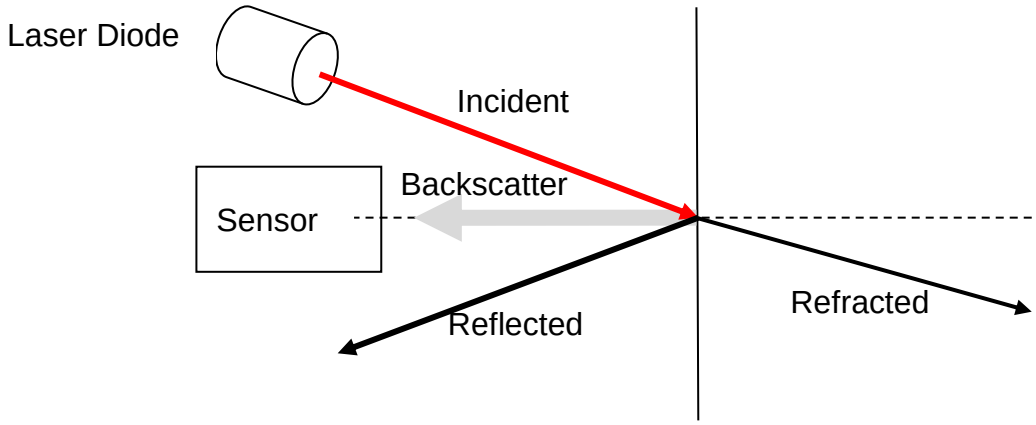

Figure 4.6 Optical test station schematic

The station was then covered up by a box, which was painted mat black on the inside to stop the light from environment affecting the sensor.

Figure 4.7 and Figure 4.8 show the configuration of the optical station. The former depicts the optical station set up, and the latter shows the station covered by the wooden box.

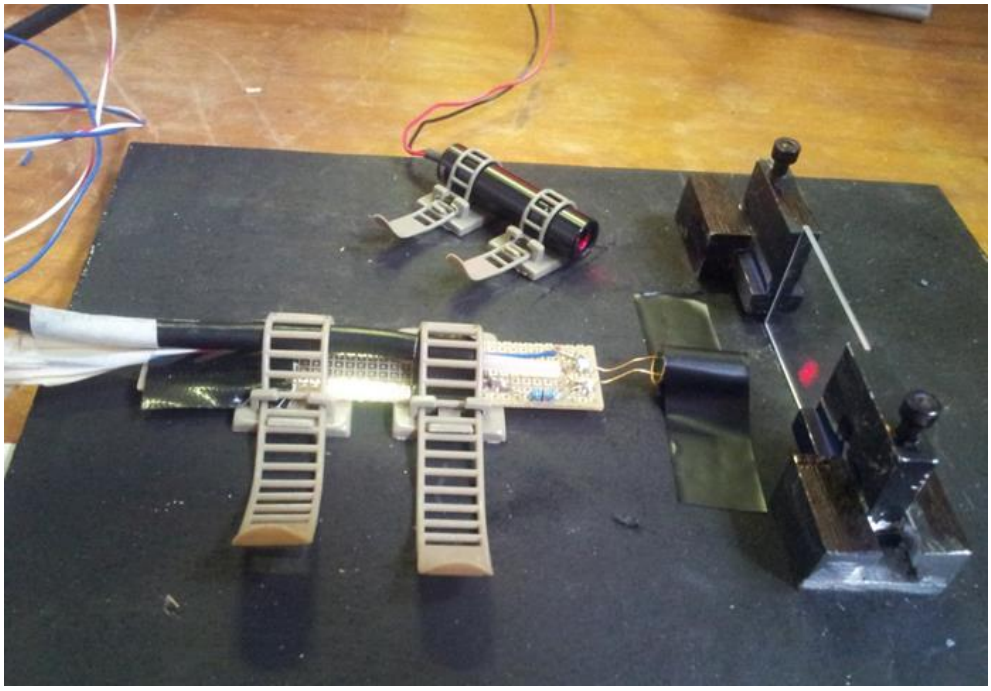

Figure 4.7 - Optical station configuration.

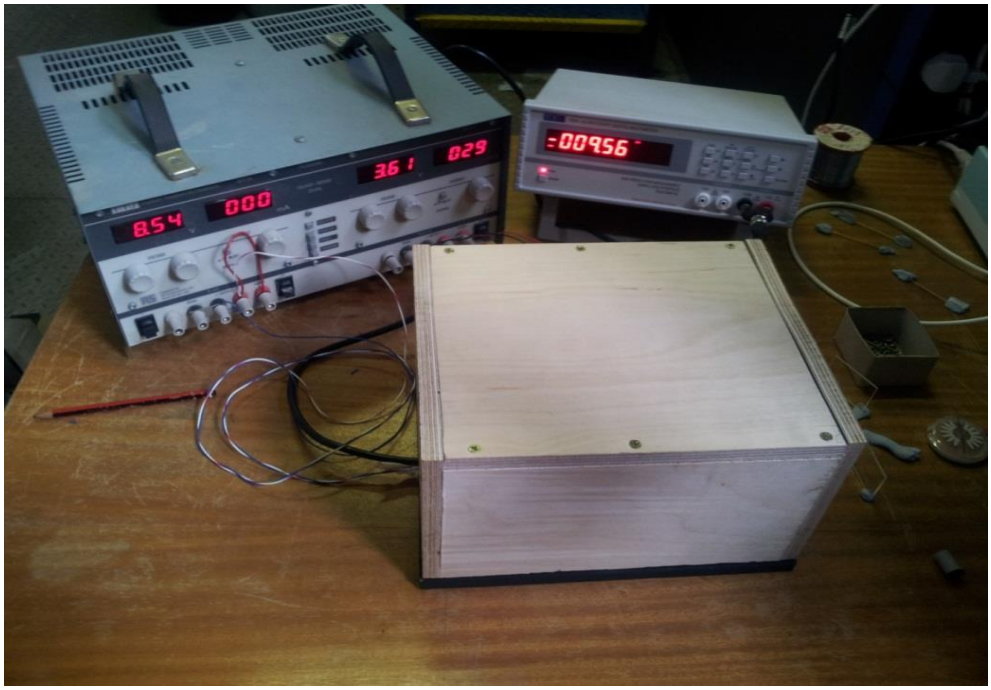

Figure 4.8 - Optical station with the box covering the samples.

4.2 Experiment Objective

The main purpose of performing the experiment was to compare the dust build up on each type of the window material. This would help with finding out which of the window samples will be a more suitable product for the DANIELA project, in terms of optical clarity. The test was to be done in two stages.

In the first stage, a preliminary test (test 1 and 2) was carried out using microscope slides. Performing the preliminary test was to help with observing the distribution of dust on the windows and how uniform the dust build up is.

In the second stage testing (test 3), actual window samples were used to assist in examining whether the amount of dust build up is different on each material.

Each sample was also tested in the optical station to enable the comparison of the optical clarity.

The testing procedures are explained in details in section 4.3.

4.3 Experiment Set up

To start with, a preliminary test (test 1 and test 2), was carried out with microscope slides. The slides were fitted onto the top wall of the icing tunnel for three weeks to confirm whether there is consistency in terms of dust build up on each individual sample.

For the purpose of this project, ambient aerosol was used. The advantage of using ambient aerosol is that it eliminates the need for the use of filters or a closed system. The dust can then be returned to the environment without any risk to people or the surrounding environment. However, this results in the aerosol particles to be uncontrolled and random. There will not be any means of knowing the material and the sizes of the particles collected on the samples.

The test was performed in the icing tunnel lab, based at Cranfield University campus in Bedfordshire. These tests were carried out between the months of January 2011 until May 2011.

The dust collected could be a mix of the following categories of aerosol:

1) Urban pollution from cars or planes (as a result of Cranfield Airport being in a short distance from the lab).

2) Fuel burning for the operation of the icing tunnel

3) Natural aerosol from trees and the dust from the ground

Figure 4.9 shows the average weather information for Cranfield, taken from the Met Office website. Although the table shows the weather average between the years 1981 to 2010, it is still a good indication of the weather average around the time of the experiment.

Woburn (Nearest climate station to Cranfield)
Climate period: 1981-2010

Station: Woburn | District: East Anglia | Region: England S | UK

Month	Max. temp (°C)	Min. temp (°C)	Days of air frost (days)	Sunshine (hours)	Rainfall (mm)	Days of rainfall >= 1 mm (days)	Monthly mean wind speed at 10m (knots)
Jan	7.0	1.3	10.4	52.0	54.2	11.6	n/a
Feb	7.4	0.9	11.4	69.4	41.7	9.3	n/a
Mar	10.3	2.7	7.0	105.5	45.3	10.6	n/a
Apr	13.1	3.8	4.5	147.4	52.1	10.2	n/a
May	16.6	6.5	1.2	183.4	54.3	8.7	n/a
Jun	19.6	9.4	0.0	179.9	53.2	9.2	n/a
Jul	22.1	11.7	0.0	197.1	53.1	8.3	n/a
Aug	21.9	11.6	0.0	189.0	55.4	8.8	n/a
Sep	18.7	9.6	0.1	137.0	57.5	9.5	n/a
Oct	14.4	7.0	2.0	105.6	70.3	10.8	n/a
Nov	10.0	3.8	5.9	61.7	63.0	10.8	n/a
Dec	7.2	1.5	10.8	43.5	57.3	10.7	n/a
Annual	14.1	5.8	53.2	1471.6	657.4	118.6	n/a

Climate period: 1981-2010

Please note that station averages are only available for 1981-2010.

Averages are available for official Met Office stations only.

All values are given to one decimal place. For 'Days of' elements, 0.1 equates to one day every ten years, 0.5 to one day every two years, 2.5 to five days every two years, and so on.

Please note that units of measurement shown may not reflect those chosen in customise settings e.g. Temperature is given in °C.

Cranfield site information:
Location: 52.070, -0.627
Altitude: 109 m above mean sea level

Woburn site information:
Location: 52.017, -0.600
Altitude: 89 m above mean sea level
Distance: 6.2 km from Cranfield

Figure 4.9 - Average weather table for Cranfield.

After the window samples were tested in the icing tunnel, the change in the samples was studied via two methods:

- Observing the results under a microscope and comparing the slides.
- Placing the window samples in the optical station and measuring the change in voltage across the resistor, as a result of the back scatter light from the microscope slides, emitted by laser.

In order to see the difference in the voltage after the windows had been placed in the icing tunnel, microscope slides were tested in the optical station in their original form and the results were recorded. They were then smeared with environment dust and grease in separate occasions; the results for each of these occasions were also recorded, as it can be seen in Table 4-2**.** This was both to have a base point to compare to and also to see if the optical system is responding and whether the change in the readings is noticeable. Table 4-2 shows the value for $V_{r,}$ for the microscope slides.

Table 4-2 Optical results from preliminary test of microscope slides.

Material	Condition	Voltage read (v)
Microscope slide	Clean	0.0014
Microscope slides	Smeared by Vaseline	0.0070
Microscope slides	Covered by eye shadow	0.0084
Microscope slides	After being cleaned by a piece of cloth	0.0014
Microscope slides	Exposed to environment dust	0.0014

To start, 6 microscope slides were placed on an aluminium plate and placed on the top wall of the icing tunnel as shown in Figure 4.10. The plate was fixed to the top of the icing tunnel, 50cm from the entrance of the icing tunnel. This was to ensure that the flow is stable as it goes over the samples. The edges of the plate were smoothened to prevent disturbing the flow any further. Figure 4.11 shows the position of the plate in the icing tunnel.

Figure 4.10 Test samples placed e in the icing tunnel.

Figure 4.11 View from the working sections of the icing tunnel.

4.3.1 Test 1

The first test was performed with 6 clean microscope slides (see Figure 4.11) for a period of 21 days and the samples were exposed to air and water for 5 hours and 57 minutes within the icing tunnel.

Table 4-3 shows the conditions under which the icing tunnel was running and the time periods during which the samples were placed in the icing tunnel.

Table 4-3 - Test 1 conditions.

Sample	microscope slides
Time period	21 days
Time exposed	5 hours and 57 minutes
Temperature	-10°C to -15°C
Water pressure	17 and 17.3 kPa

Air pressure	24 kPa
Speed	50 m/s

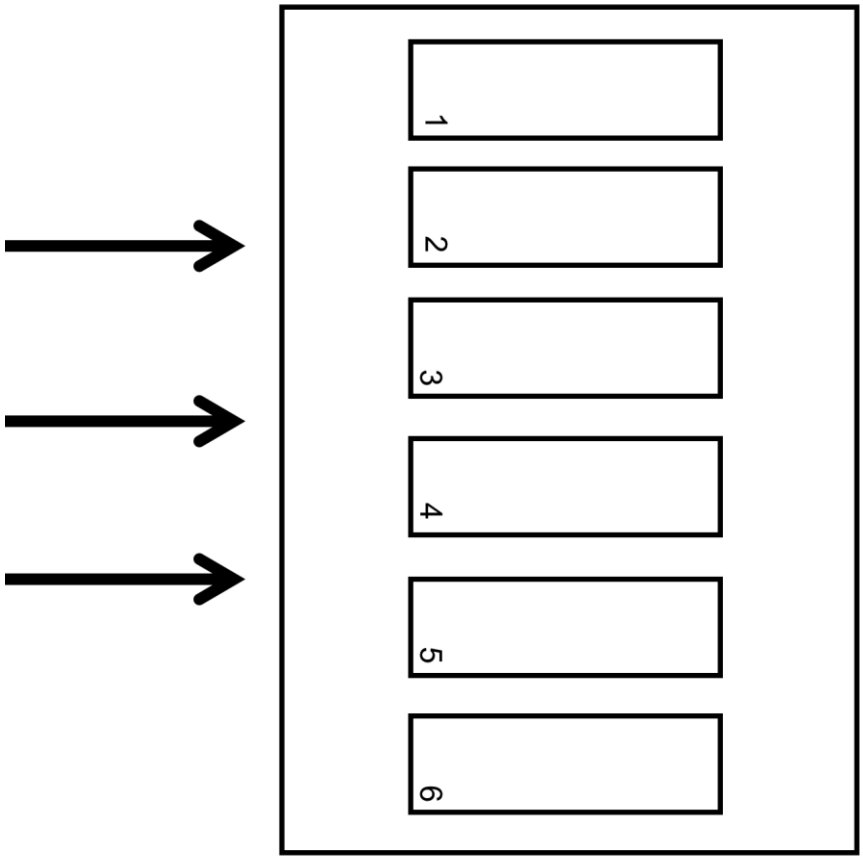

Figure 4.12 The position of slides.

The order of the samples placed in the icing tunnel is shown in Figure 4.12. The samples were then taken out and tested. While taking out the samples, care was taken to avoid any contact with the samples and to keep these as undisturbed as possible.

Table 4-4 - Optical results from test 1

Sample numbers	Voltage reading (v)
1	0.004
2	0.004
3	0.008
4	0.007
5	0.011
6	0.012

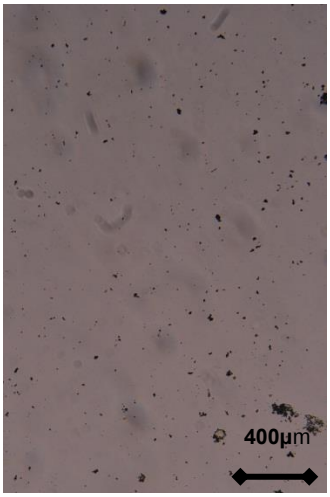

Slide 1

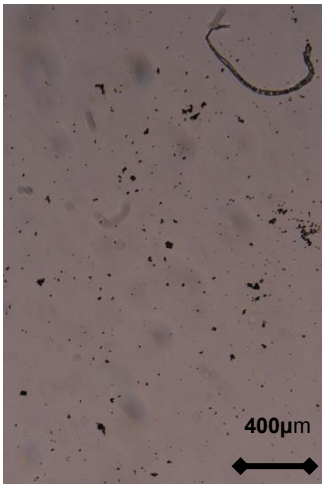

Slide 2

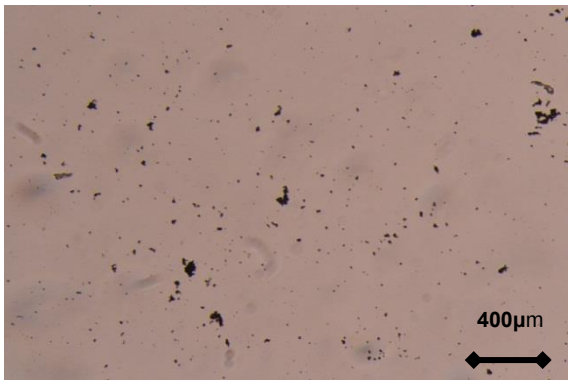

Slide 3

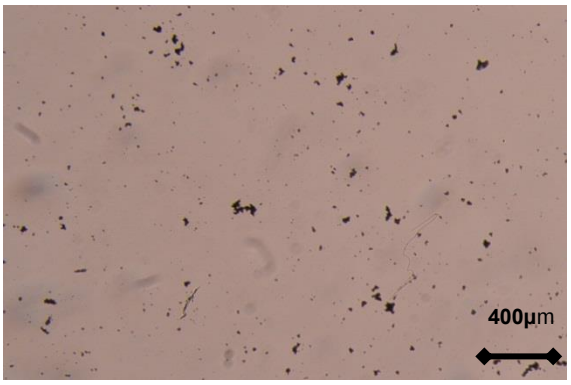

Slide 4

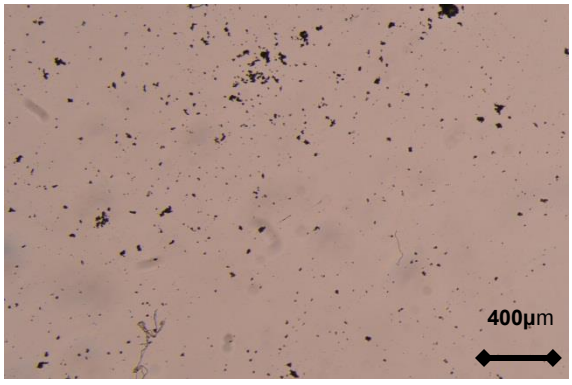

Slide 5

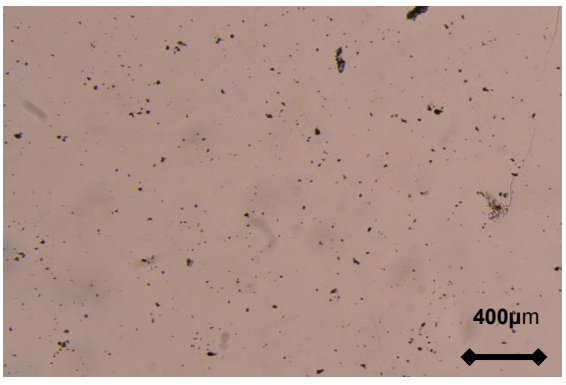

Slide 6

Figure 4.13 - Microscope slides placed under the microscope.

4.3.2 Test 2

A similar test was carried out for another set of samples. The samples were in the icing tunnel for a total of 9 hours in a period of 3 days.

Table 4-5 - Test Condition for test 2

Sample	Microscope slides
Time period	4Days
Time exposed	9 hours
Temperature	-10°C to -15°C
Water pressure	17 - 17.3 kPa
Air pressure	24 kPa
Speed	50 m/s

Table 4-6 Optical test results for test 2

Sample numbers	**Voltage reading (v)**
1	0.00014
2	0.00014
3	0.00014
4	0.00014
5	0.00014
6	0.00020

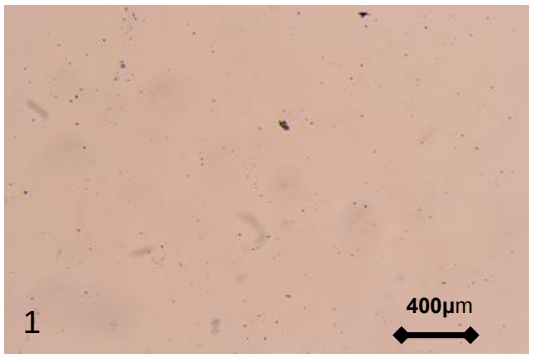

Slide 1

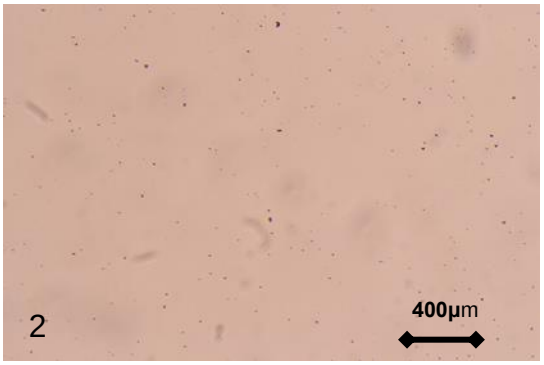

Slide 2

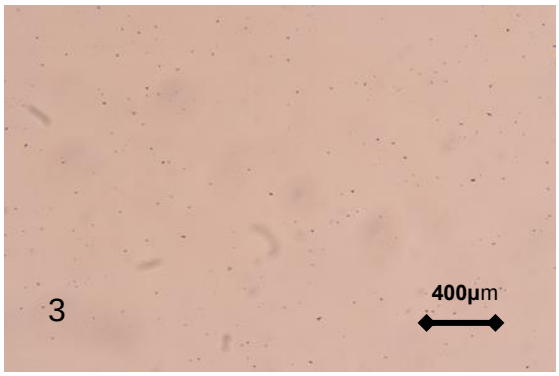

Slide 3

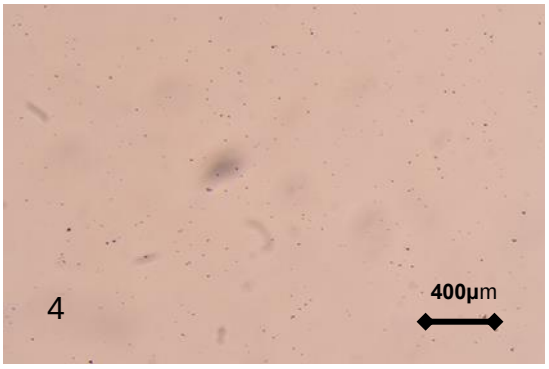

Slide 4

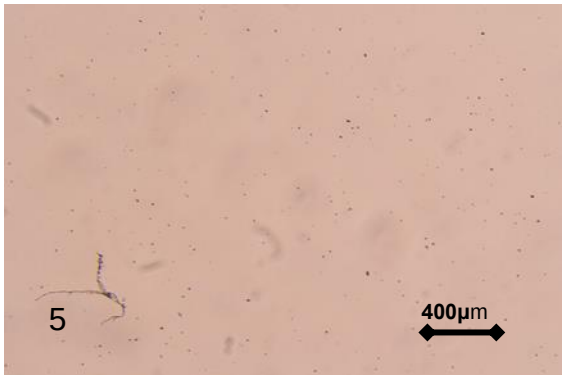

Slide 5

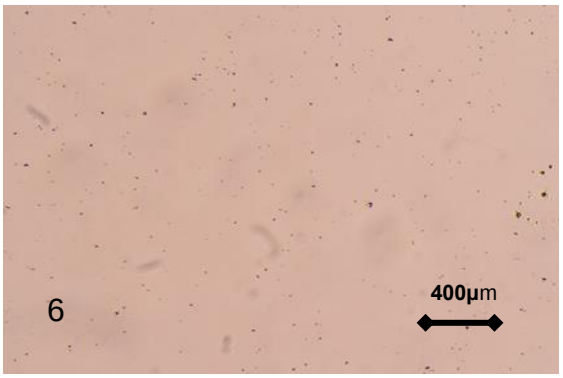

Slide 6

Figure 4.14 - Microscope observation of the window samples.

From the preliminary tests (test 1 and 2), it can be seen in test 2 results, there has not been much dust particles collected on the windows. This shows that the time period the samples are exposed to dust can have a great effect on the number of particles attached to the surface.

However it can be determined that the samples placed within the icing tunnel at the same time and under the same condition have collected almost the same amount of dust while in the icing tunnel and there is consistency in the results.

4.3.3 Test 3

After completing the preliminary tests (test 1 and 2) and confirming the consistency in the adhesion of dust on all the samples, the window samples were placed in the icing tunnel.

The test samples were placed in the optical station to measure the change in voltage before being placed in the icing tunnel. The results were as follows:

Table 4-7 - Optical test for the window samples before being exposed to dust

Sample numbers	Voltage reading (v)
1 – Microscope slide	0.00014
2– BK7	0.00031
3 - Sapphire	0.00011
4 - Germanium	0
5 - Zns	0.00761
6 – Microscope	0.00014

The test samples were placed in the icing tunnel in the order shown in Figure 4.15.

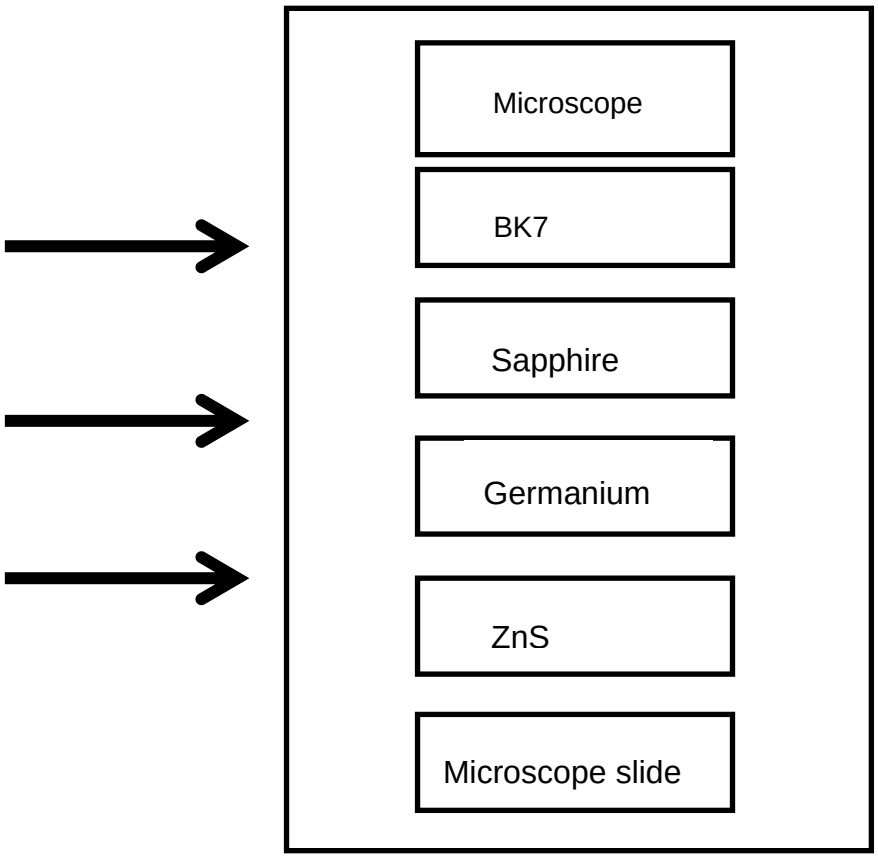

Figure 4.15 - Placement of the window samples.

The samples were in the icing tunnel for a period of 12 hours and 47 minutes over 21 days. Table 4-8 shows the test conditions and Table 4-9 shows the test results after placing the test samples in the optical station.

Table 4-8 - Test conditions for window sample – test 3

Sample	Actual samples
Time period	21 days
Time exposed	12 hours and 47 minutes
Temperature	-10°C to -15°C
Water pressure	17-17.3 kPa
Air pressure	24 kPa
Speed	50 m/s

Table 4-9 - Optical rest result for the window samples – Test 3

Sample numbers	First voltage reading (v)	Second voltage reading (v)
1 – Microscope slide	0.00074	0.00074
2 – BK7	0.00031	0.00040
3 - Sapphire	0.00032	0.00037
4 - Germanium	0.00125	0.00126
5 - Zns	0.00793	0.00779
6 – Microscope	0.00081	0.00079

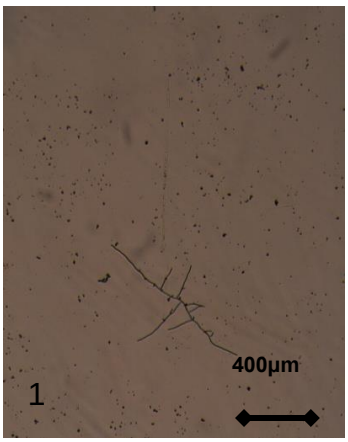

Slide 1

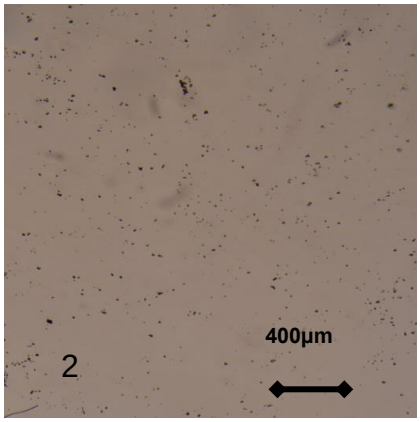

Slide 2

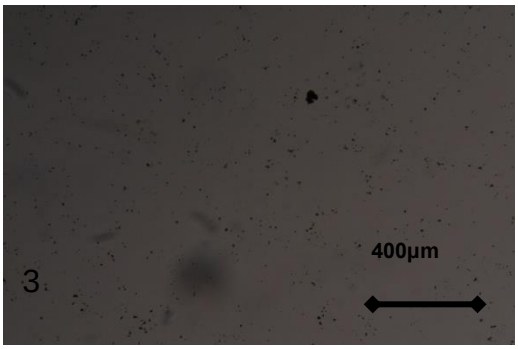

Slide 3

Slide 4

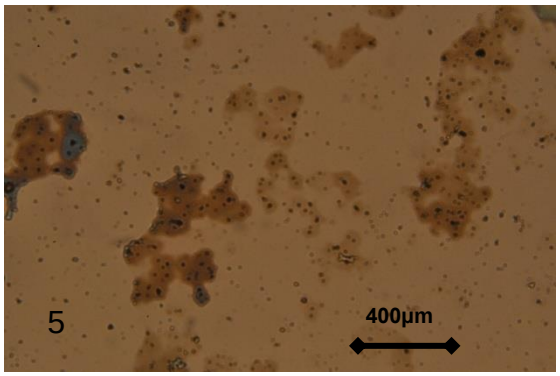

Slide 5

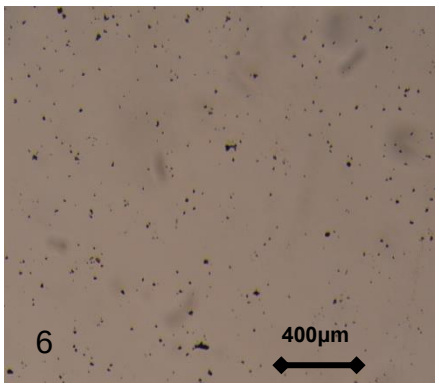

Slide 6

Figure 4.16 - Microscopic observation of window samples.

4.4 Experimental Results

As it can be seen from the data gathered from both the optical tests and the visual analysis under the microscope, it is clear that under the same conditions, the amount of dust particles collected varies on the surface of different materials.

From the preliminary tests (test 1 and 2), it can be seen that samples collected more dust in test 1 in comparison with test 2. This shows that the time period the samples are exposed to dust can have a great effect on the number of particles attached to the surface.

From test 3, it can be seen that BK7 and sapphire gave the same results; however Zinc Sulphite has collected considerably more dust on the surface. Compare to these microscope slides which were tested, are in the middle position, they collect noticeably less dust compare to Zinc Sulphite and slightly more dust in comparison with BK7 and Sapphire.

Under the current set up, it is impossible to optically test the Germanium or observe the specimen under the microscope. Germanium is opaque in the visible spectrum, specifically at the wavelength of the laser and any dust collected on the sample cannot be seen on the surface using a microscope. However Germanium is transparent in both long wave (8-12μm) and short wave (3-5μm).

Table 4-10, summarises the results achieved for each test sample.

Table 4-10 – Material comparison

Samples	Material class	Some relevant qualities	Average voltage reading (v)	Dust collection comparison - Microscope observation (1 = lowest amount of dust collected - 3 = Highest amount collected)
Microscope slide	Glass	-	0.00074	2
BK7	Glass	high homogeneity and low bubble content	0.000355	1
Sapphire	Single crystal	survives in challenging environments	0.000345	1
Germanium	Single crystal	to increase the windows strength and durability	0.001255	-
Zns	Polycrystalline	weak against erosion and requires a protective coating	0.00786	3

CHAPTER 5. CONCLUSIONS

The objective of this work was to compare the optical clarity of a number of available optical window materials suitable for the DANIELA project.

To observe whether an optical window of a specific material will collect more dust compared to others under the same conditions. This was achieved by testing the window samples in the icing tunnel and leaving them for a number of hours exposed to wind and water and atmospheric aerosol particles. The samples were studied under the microscope. They were also placed in the optical station which was designed to show the change in voltage across the sensor, caused by back scattered light from the dust particles adhered to the samples.

The results from the optical station verify the observation under the microscope. The higher the voltage obtained from the optical station, the more dust collected on the samples.

Results from both tests proved that under the same test conditions, i.e. flow, temperature and moisture, the BK7 and Sapphire collect considerably less dust in comparison with the Zinc Sulphite and the microscope slides. Zinc Sulphite however collects more dust compared to the other samples.

Germanium could be tested neither optically nor under a microscope as it is a dark opaque material.

To recommend one of these samples as a solution for the air data system however requires more research and work. The recommendation for this has been included in the next chapter.

CHAPTER 6. RECOMMENDATION FOR FUTURE WORK

The test performed within the icing tunnel can be extended further by building a test rig as based on the information and design specifications included in this thesis.

The experiment can then be further extended to compare the effects of different variables on the adhesion of particles to the windows. Some of these variables are: particle size and shape, static electricity, relative humidity and the flow movement. Some of these effects can be studied as follows:

As discussed in the literature review bouncing does not occur for droplets or easily deformed particles. Harder particle materials, larger particle size and greater velocity increase the probability of bouncing. Therefore to expand on the work completed particles size and shape can be tested by introducing other types of particles or droplet to the flow in a controlled manner, for example, oil droplets or smoke particles. For this purpose I would recommend a PivPart droplet generator which would create droplets of specific size, and Arizona dust as solid particles.

Another factor which could be studied further is the surface quality. Coating surfaces with oil or grease increases the adhesion energy, the deformation and the dissipative energy and greatly reduces the possibility of bouncing. This can be tested further by manipulating the surface of the samples via application of oil or grease to the surface or examine different coating options available for different materials tested.

Aerosol particles carry some electric charge. This results in the particles adhering to the surface as the electrical charge can overcome the other forces such as gravity. Static electricity can be tested by charging the plate which holds the window samples or charging the particles.

Experimental work performed by different scientists show that the relative humidity of the ambient air affects the adhesion of solid particles to solid

surfaces. To study the effects of humidity on adhesion, the test can be analysed by running the tunnel on a rainy day and a dry day to compare the effect of humidity on the adhesion process.

Effects of boundary layer thickness could be studied as part of the future work. As reviewed in the Section 1.1 of the report particles smaller than the boundary layer are in part protected from re-entrainment by being submerged in the boundary layer, therefore, reducing the chance of a particle being detached from the surface by stream of air. To examine this, boundary layer can be tripped, by placing a wooden block before the windows to see if the change in the flow will have any effects on the adhesion. For this purpose, the windows can also be placed in a way that there will be a small gap between the edge of the plate and the edge of the windows.

Other materials could be considered. Some of these materials are:

- Silicon: Silicon is a good mid wave optical material. However, it is highly reflective, and needs anti-reflective coating and it has a modest sand and rain erosion.
- Fused Quartz: Callister (2003) explains that there are three polymorphic crystalline forms of Silica; and quartz is one of them. The structure of these materials is relatively complicated and the atoms are not positioned close to each other. This results in a low density value. Moreover, Fused quartz displays strength, and has the ability to remain stable under high temperatures. It also has a high resistivity.

Germanium was not tested and analysed, with the existing set up as it is impossible to optically test or observe the specimen under the microscope. Germanium is however transparent in both long wave (8-12μm) and short wave (3-5μm) and it can be tested using Infra red laser.

REFERENCES

1. AvÅŸar, A. Levent et al. "Development and Verification of High-Durability Infrared Transparent Coating for Airborne Usage". *Current Developments in Lens Design and Optical Engineering XI; and Advances in Thin Film Coatings VI* 7786 (2010): n. pag. Web. 2 Feb. 2016.
2. Blaire, Gordon, and Melvin Cahoon. *Special Investigation: Design of an Intake Bell Mouth*. 2016. Print.
3. Bohren, Craig F, and Donald R Huffman. *Absorption and Scattering of Light by Small Particles*. New York: Wiley, 1998. Print.
4. Bowden, Frank Philip, and David Tabor. *The Friction and Lubrication of Solids*. Oxford: Clarendon Press, 2001. Print.
5. Callister, William D. *Materials Science and Engineering*. New York: John Wiley & Sons, 2007. Print.
6. CÌ§engel, Yunus A, and Robert H Turner. *Fundamentals of Thermal-Fluid Sciences*. Boston: McGraw-Hill, 2001. Print.
7. Corn, Morton, and Felix Stein. "Re-Entrainment of Particles from a Plane Surface". *American Industrial Hygiene Association Journal* 26.4 (1965): 325-336. Web. 2 Feb. 2016.
8. Corn, Morton. "The Adhesion of Solid Particles to Solid Surfaces II". *Journal of the Air Pollution Control Association* 11.12 (1961): 566-584. Web. 2 Feb. 2016.
9. Corn, Morton. "The Adhesion of Solid Particles to Solid Surfaces, I. A Review". *Journal of the Air Pollution Control Association* 11.11 (1961): 523-528. Web. 2 Feb. 2016.
10. Cranfield.ac.uk, "Icing Tunnel". N.p., 2016. Web. 23 Feb. 2016.
11. Dahneke, Barton. "The Capture of Aerosol Particles by Surfaces". *Journal of Colloid and Interface Science* 37.2 (1971): 342-353. Web. 2 Feb. 2016.
12. Daly, B. B. *Woods Practical Guide to Fan Engineering*. [Colchester]: Woods of Colchester Limited, 1978. Print.
13. Esmen, Nurtan A., Paul Ziegler, and Robert Whitfield. "The Adhesion of Particles upon Impaction". *Journal of Aerosol Science* 9.6 (1978): 547-556. Web. 2 Feb. 2016.

14. Friedlander, Sheldon K. *Smoke, Dust, and Haze*. New York: Oxford University Press, 2000. Print.
15. Gardos, Michael N., Bonnie L. Soriano, and Steven H. Propst. "Study On Correlating Rain Erosion Resistance With Sliding Abrasion Resistance Of DLC On Germanium". *Diamond Optics III* 1325 (1990): n. pag. Web. 2 Feb. 2016.
16. Harris, Allison R., and Cliff I. Davidson. "Particle Resuspension in Turbulent Flow: A Stochastic Model for Individual Soil Grains". *Aerosol Science and Technology* 42.8 (2008): 613-628. Web. 2 Feb. 2016.
17. Harris, Daniel C. *Materials for Infrared Windows and Domes*. Bellingham, Wash.: SPIE, 1999. Print.
18. Hinds, William C. *Aerosol Technology*. New York: Wiley, 1999. Print.
19. Hudson, Martin D. et al. "Fabrication and Testing Of Diamond Coatings on Infrared Windows for the Harrier GR7 and AV8-B Systems". *Window and Dome Technologies and Materials V* (1997): n. pag. Web. 2 Feb. 2016.
20. Jin, C., I. Potts, and M. Reeks. "A Simple Stochastic Quadrant Model for the Transport and Deposition of Particles in Turbulent Boundary Layers". *Physics of Fluids (1994-present)* 27.5 (2015): 053305. Web. 2 Feb. 2016.
21. Massey, B. S. *Mechanics of Fluids*. Wokingham, Berkshire, England: Van Nostrand Reinhold (UK), 1983. Print.
22. Met Office,. "Weather and Climate Change". N.p., 2016. Web. 2 Feb. 2016.
23. Optical Materials Overview,. "CVI Laser Technical Notes". N.p., 2016. Web. 2 Feb. 2016.
24. Osborne, S.R., and J.M. Haywood. "Aircraft Observations of the Microphysical and Optical Properties of Major Aerosol Species". *Atmospheric Research* 73.3-4 (2005): 173-201. Web. 2 Feb. 2016.
25. Pepi, John. "Fail-Safe Design of an All BK-7 Glass Aircraft Window". *Window and Dome Technologies and Materials* 2286 (2016): n. pag. Web. 2 Feb. 2016.
26. Phares, Denis J, Gregory T Smedley, and Richard C Flagan. "EFFECT OF PARTICLE SIZE AND MATERIAL PROPERTIES ON AERODYNAMIC RESUSPENSION FROM SURFACES". *Journal of Aerosol Science* 31.11 (2000): 1335-1353. Web. 2 Feb. 2016.

27. Pruszynski, Charles J. et al. "Design, Fabrication, and Testing Of Large Airborne Znse Windows". *Optical Manufacturing and Testing* (1995): n. pag. Web. 2 Feb. 2016.
28. Rabinovich, Yakov I. et al. "Adhesion between Nano-scale Rough Surfaces". *Journal of Colloid and Interface Science* 232.1 (2000): 10-16. Web. 2 Feb. 2016.
29. Ranade, M. B. "Adhesion and Removal of Fine Particles on Surfaces". *Aerosol Science and Technology* 7.2 (1987): 161-176. Web. 5 Feb. 2016.
30. Reeks, Mike. "Peer Review of the Methodology for Calculating the Transport and Deposition of Dust in AGR Circuit". (2016)
31. Reeks, M. W. and Hall, D. “Kinetic Models for Particle Resuspension in Turbulent Flows: Theroy and Measurement”, Journal of Aerosols Science 32 1-31, (2001)
32. Schick, M. J. "Introduction to Aerosol Science, Parker C. Reist, Macmillan, New York, 1984, 299 Pp. Price: $38.00". *Journal of Polymer Science: Polymer Letters Edition* 23.3 (1985): 162-163. Web. 2 Feb. 2016.
33. Schuhmann, Rainer. "Standardized Optical Components For Laser Applications". *Design and Engineering of Optical Systems II*. Berlin 2016
34. Sorato, Sebastiano. "Methodology to Analyse Three Dimensional Droplet Dispersion Applicable To Icing Wind Tunnels". PhD. Cranfield University, 2009. Print.
35. Sullivan, Roger M. "A Historical View Of Germanium As An Infrared Window Material". *Window and Dome Technologies and Materials XI* 7302 (2009): n. pag. Web. 2 Feb. 2016.
36. Teem Photonics,. *Report On Environmental Testing*. 2016. Print. DANIELA Project.
37. Telling, Robert H., G. H. Jilbert, and John E. Field. "Erosion Of Aerospace Materials By Solid-Particle Impact". *Window and Dome Technologies and Materials V* (1997): n. pag. Web. 2 Feb. 2016.
38. Thornton, Colin, and Zemin Ning. "A Theoretical Model For The Stick/Bounce Behaviour Of Adhesive, Elastic-Plastic Spheres". *Powder Technology* 99.2 (1998): 154-162. Web. 2 Feb. 2016.

39. Tu, Jiyuan, Guan Heng Yeoh, and Chaoqun Liu. *Computational Fluid Dynamics*. Amsterdam: Butterworth-Heinemann, 2008. Print.
40. Vincent, James H. *Aerosol Sampling*. Chichester, England: John Wiley & Sons, 2007. Print.
41. Wang, Hwa-Chi. "Effects of Inceptive Motion on Particle Detachment from Surfaces". *Aerosol Science and Technology* 13.3 (1990): 386-393. Web. 2 Feb. 2016.
42. Winker, David M. et al. "Overview of the CALIPSO Mission and CALIOP Data Processing Algorithms". *J. Atmos. Oceanic Technol.* 26.11 (2009): 2310-2323. Web. 2 Feb. 2016.
43. Winkler, Peter. "Relative Humidity And The Adhesion Of Atmospheric Particles To The Plates Of Impactors". *Journal of Aerosol Science* 5.3 (1974): 235-240. Web. 2 Feb. 2016.
44. Wood, N.B. "A Simple Method For The Calculation Of Turbulent Deposition To Smooth And Rough Surfaces". *Journal of Aerosol Science* 12.3 (1981): 275-290. Web. 2 Feb. 2016.
45. Wu, Chuan-yu, Long-yuan Li, and Colin Thornton. "Rebound Behaviour of Spheres For Plastic Impacts". *International Journal of Impact Engineering* 28.9 (2003): 929-946. Web. 2 Feb. 2016.
46. Yadagiri, Srinivas Rao, and Ronian Siew. "Influence Of Coating Stress Of Diamond-Like Carbon Coating On Surface Flatness Of Large Germanium Windows". *Optical Components and Materials IX* 8257 (2012): n. pag. Web. 2 Feb. 2016.
47. Zimon, A. D. *Adhesion Of Dust And Powder*. New York: Plenum Press, 1969. Print.

Appendix A - Fan Specifications

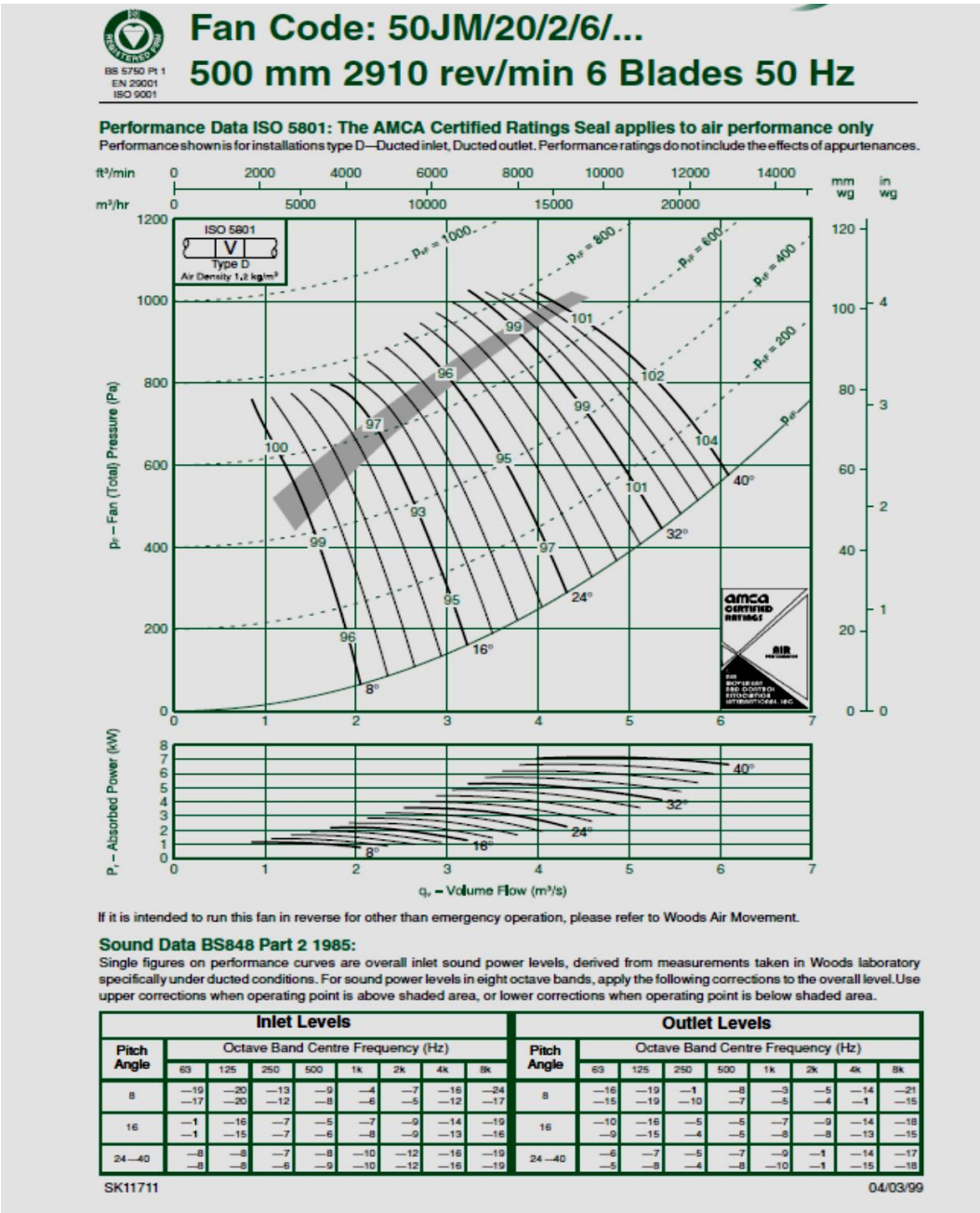

Figure A.1 - Fan specification

The following pictures were taken while testing DANIELA windows in the icing tunnel at Cranfield.

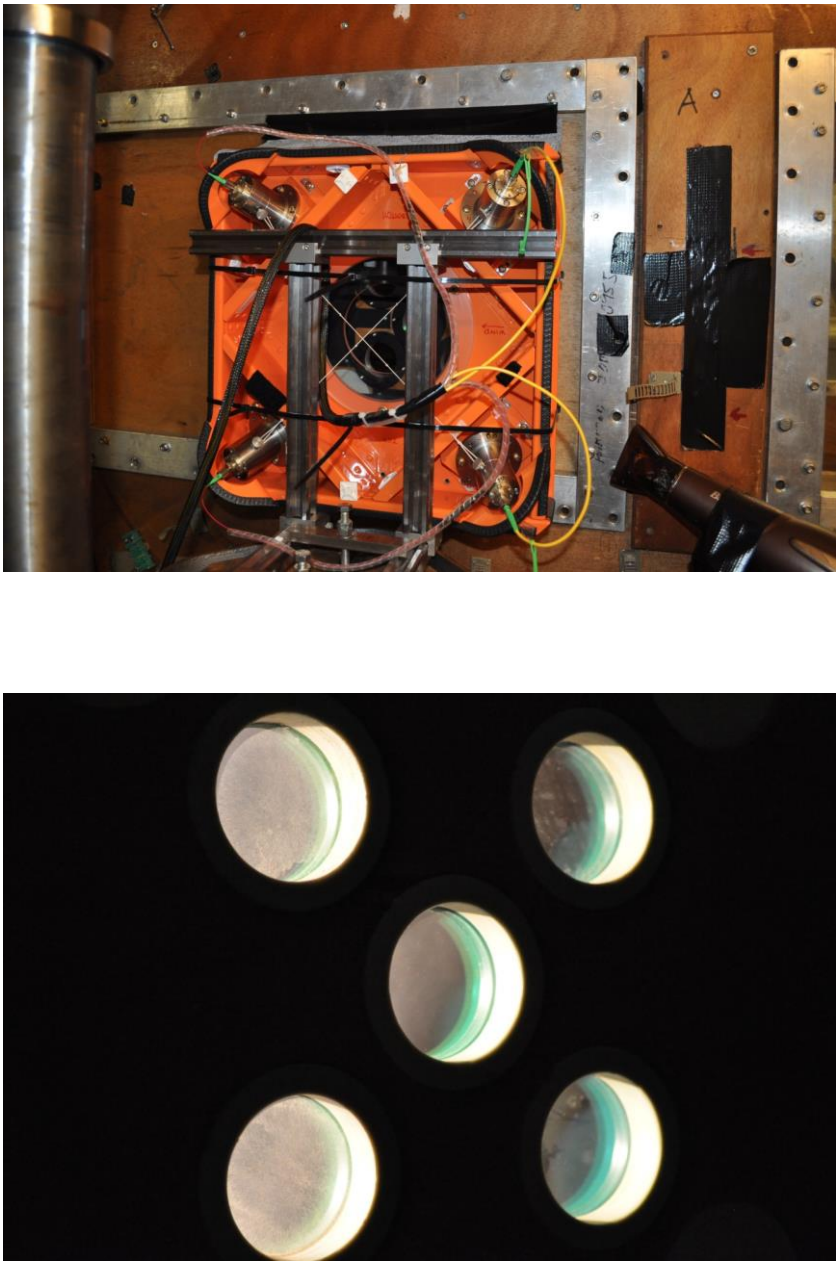

Figure A.2 - DANIELA window.